# Enable Placental Extracellular Vesicle Isolation Using Binary Temperature-responsive Reagent System

Zirui Fu

A thesis

submitted in partial fulfillment of the

requirements for the degree of

Master of Bioengineering

University of Washington

2020

Reading Committee:

James Lai

Lucia Vojtech

Program Authorized to Offer Degree:

Bioengnieering

University of Washington

**Abstract**

Enable Placental Extracellular Vesicle Isolation Using Binary Temperature-responsive Reagent System

Zirui Fu

Chair of the Supervisory Committee:

James Lai

Bioengineering

Extracellular vesicles (EVs) are cell-secreted lipid bilayer vesicles which play important roles in human cell signaling. In recent years, the researches regarding the placenta derived EVs which are secreted from the syncytiotrophoblast (STB), have discovered the potentials of placental EVs as a novel non-invasive marker for monitoring placental development and functions in real time. With specific STB markers, principally placental alkaline phosphatase (PLAP), we can distinguish STB-derived EV (STBEV) from those produced by other cell types. Due to the complexity of pregnancy plasma sample, we propose the binary temperature-responsive reagent system for fast and specific isolation of $PLAP^+$ EV from pregnancy plasma. The proposed binary reagent system consists of temperature-responsive conjugate and magnetic nanoparticles. The synthesis of the conjugate included the polymerization of temperature-responsive poly(N-

isopropylacrylamide) (pNIPAAm) via Reversible addition-fragmentation chain transfer (RAFT) and the conjugation of synthesized pNIPAAm with antibody. $^{1}$H NMR was used to confirm the composition of pNIPAAm and the GPC characterization showed the number average molecular weight (Mn) of the synthesized pNIPAAm was 29070 with a polydispersity index (PDI) at 1.186. The polymer-antibody conjugation was characterized by SDS-PAGE, which confirmed the optimal polymer/antibody molar ratio was 200:1. While tested on fluorescent proteins, the resulting conjugates stably achieved over 90% target protein capture while applying 10:1 conjugate/target molar ratio. To demonstrate the practical utilities of binary reagent system on placental EV separation, we used PLAP antibody to perform purified placental EV separation and pregnancy plasma separation. Digital Droplet PCR (ddPCR) and RT-PCR characterizations confirmed the specific placental EV isolation from pregnancy plasma by PLAP antibody via binary reagent system.

# TABLE OF CONTENTS

Seminal EV separation by targeting tetraspanins..... 53

# ACKNOWLEDGEMENTS

The author thanks Dr. James Lai, Dr. Lucia Vojtech, Dr. Selvi Srinivason, Dr. Patrick Stayton, Pinar Calis, M Vatich, C Redman, Dr. Michael G Gravett for providing materials, working space and help on experiment. Financial support was provided by NIH HD089670.

# Chapter 1. EXTRACELLULAR VESICLES

Extracellular vesicles (EVs) are lipid bilayer vesicles secreted by cells. EVs are cargos of nucleic acids, proteins, lipids or metabolites from their parent cells. Over the years, researchers have identified various subtypes of extracellular vesicles based on their size and origin. Generally, extracellular vesicles can be categorized into 3 main classes: exosomes, microvesicles and apoptotic bodies.

Exosomes are the EVs originated from endocytic pathway in healthy cells, they are released upon fusion of multi-vesicular bodies with the plasma membrane. The size of exosomes typically ranges from 40 to 120nm. Microvesicles are the EVs originated from outward budding of healthy cell plasma membrane. The size of microvesicles has a wider range, starting from 50nm to 1000nm.[1, 2] During apoptosis of apoptotic cells, the apoptotic bodies are produced from the outward blebbing of cells' membrane. The materials sealed in the apoptotic bodies can be delivered to other healthy recipient cells. The size of apoptotic bodies can range from 500 to 2000nm.[3]

While the nucleic acids cargoes in EVs are highly dictated by their parent cells, several types of proteins remain relatively conservative over various exosomes and microvesicles. Because of their endocytic origin, some particular proteins are commonly enriched in endosome, including

Rab GTPases, SNAREs, Annexins, flotillin, etc. Some of these proteins such as Alix and Tsg101 are involved in multivesicular endosomes biogenesis and are normally used as exosome markers. Tetraspanins (e.g. CD63, CD81, CD9) are a family of more than 30 proteins that are composed of four transmembrane domains, known to cluster into microdomains at the plasma membrane. Tetraspanins, especially CD63, CD9 and CD81, are common exosomal surface markers. Microvesicles are having a wider range of size and protein cargoes, common protein markers used to define microvesicles are selectins, integrins and the CD40 ligand.[4]

## 1.1 Significance of Extracellular Vesicles

Although the intercellular communication in multicellular organisms has been studied for a long time, it is in the last two decades that researchers start to appreciate the EVs secreted from healthy cells are playing an important role in intercellular communication.[4]

The functions of EVs in human cell signaling can be broad, such as immune suppression, inflammation, coagulation and so on. For example, tumor-derived exosomes can carry a cargo of negative immunoinhibitory molecules and signal factors to immune cells for re-programming their functions.[5] The secretion of choroid plexus epithelial cells-derived, miRNA-containing EVs which carry specific miRNA molecules and proteins, can cross the ependymal cell layer lining the ventricles, reach the recipient brain parenchymal cells, trigger target mRNA repression, and induce an inflammatory response.[6] In a mice model, the EVs derived from tumor cells were

shown to deliver coagulant tissue factors to activated platelets at a site of vascular injury via interaction between P-selectin glycoprotein ligand-1 (PSGL-1) and P-selectin.[7]

So far, many applications based on EV are explored, such as EV-related diagnostics and therapies. The relative ease of sampling EVs from biological fluid and the non-invasiveness make EV-related diagnostic strategies become popular in the past decade. For example, by enriching EVs via neuronal cell surface marker L1CAM, several classical Alzheimer's disease (AD) biomarkers including Aβ42 and P-tau (phosphorylated at the S396 or T181 sites) are characterized, which provides substantial support to the early diagnoses of AD.[8] In a case-control study in 2014, the levels of Aβ42, P-S396-tau, P-T181-tau from neutral marker enriched exosomes can predict the development of AD up to 10 years before clinical onset.[9] Other than diagnostics, EVs also lead to the development of novel cell-free therapies due to their unique mechanism of interacting to target recipient cells. In some cases, the secreted EVs are fused to target cell membrane and are internalized by endocytosis with their cargoes being transferred into the new cells and staying functional.[8] In murine models, the systematic injections of exosomes secreted from immunosuppressive dendritic cells (DC) are able to suppress the inflammatory and autoimmune responses, which represents a potential EV therapy for treating autoimmune diseases.[10]

## 1.2 EV ISOLATION STRATEGIES AND CHALLENGES

At present, it is well established that EVs are playing critical role in intercellular communication, affecting various physiological process in humans, such as inflammation, cell proliferation and coagulation. The presence of EVs in various body fluids, including plasma, urine, spinal fluid, saliva, is also emphasizing the potential of EVs to provide biomarkers for diagnosis and prognosis of different diseases. However, it has long been an issue that the isolation of EVs from their biological origins is challenging due to the unique obstacles presented in different human body fluid. For example, the conventional EV isolation methods such as Ultrafiltration or Differential Centrifugation are highly limited while isolating EVs from urine. The high concentration of Tamm-Horstall protein in urine can polymerize into EV-trapping mesh, consequently, leads to the difficulties of EVs isolation from urine. Similarly, the isolation of EVs from plasma has its unique challenge associated with the plasma properties. For example, the blood samples collected on different anticoagulants, such as EDTA, citrate and heparin, when processed further downstream, could exhibit different EV yields. [11]

As a result, lacking standardized techniques to isolate EVs effectively, substantially impact the development and application of analytical approaches. Also, the conventional methodologies are time consuming and difficult to translate to clinical practice.[12] For example, the gold standard method of isolation, differential centrifugation, requires multi-step ultracentrifugation which is labor-intensive and is not ideal in specificity. Besides, the complexity of biological fluids makes it challenging to isolate a specific population of EVs since many biological components such as lipoprotein, chylomicrons, exosomes and microvesicles overlap with each other in size.[13] Other

than differential centrifugation, the mainstream strategies currently being utilized in exosomes isolation also include ultrafiltration, size exclusion chromatography, precipitation, immunoaffinity interaction and microfluidic devices (Table 1).

Table 1. Current mainstream EV isolation strategies. [14, 15]

| Strategy | Time, min | Cost | Purity | Volume, mL |
|---|---|---|---|---|
| Differential centrifugation | 140-600 | $ | Low | 10~100 |
| Ultrafiltration | 120 | $ | Low | >100 |
| Size Exclusion Chromatography | 60 | $$ | Medium | 0.1~1 |
| Precipitation | 60-120 | $ | Low | 1~10 |
| Immunoaffinity Interaction | 240 | $$$ | High | 1~10 |
| Microfluidic Device | 30 | $ | High | < 0.05 |

Differential centrifugation is the standard and classical separation method, which separates EVs based on their buoyant density by centrifugation. There are typically multiple steps of low speed centrifugation (300x g, 2000x g, 10000x g) before performing ultracentrifugation (100,000x ~ 200,000x g) in order to reduce losses caused by co-sedimentation. One main issue of ultracentrifugation is that there is no unified protocol to process different biological fluids. [14] Among different researches, the number of stages and conditions of differential centrifugation always vary widely.

Ultrafiltration is a separation method based on the size of vesicles. The vesicles populations with similar sizes are purified by porous filter. Some common pore diameter includes 0.8, 0.45, 0.22 micrometer. Even though the ultrafiltration alone is sufficient for EV isolation, it is always being used as an additional step with gel filtration method or ultracentrifugation method.[14] The challenge of this method is the potential deformation of EVs during filtration, and the contamination of different biomolecules.

Size exclusion chromatography is another filtration-based method, gel filtration. The mechanism of size exclusion chromatography to separate molecules is the samples with different hydrodynamics diameter will have different retention time in a column filled with porous resin. Though SEC provides pure EV product compared to ultracentrifugation and ultrafiltration, the input volume is limited to 5-10% of the column volume. Therefore, SEC strategy is more suitable for analytical purpose rather than scalable preparation.

Precipitation, mainly using hydrophilic polymer such as PEG, is another widely used strategy for EVs isolation. This method utilizes a decrease in the solubility of EVs in the solutions of superhydrophilic polymers, PEGs. This method becomes popular because of its simplicity, speed, compatibility for physiological pH range and weak dependence on the ion concentration.[14] However, the major issue is the contamination of co-precipitated proteins and various impurities, which make it a challenge for downstream analysis requiring high purity.

Immunoaffinity-based strategy generally utilizes the EV protein receptors as antigens and uses antibodies to specifically capture the EV population of interest. Many commercialized kits are designed based on this method with various modification, such as Dynabeads by Thermo Fisher Scientific. While immunoaffinity strategy increase the selectivity and purity of EV isolation, it also requires pricy consumables and reagents. The capacity of processing large volume and complex sample is not comparable to conventional method such as ultracentrifugation or ultrafiltration.

Microfluidic devices are relatively less popular in EVs isolation. But this method is unique in reproducing numerous laboratory processes on a microscale with a high accuracy and specificity

(lab-on-a-chip) instead of using expensive equipment. Many of the strategies described above can be integrated into microfluidic devices and be realized in the lab. But this strategy is more attractive to projects aiming at analyzing a small scale of samples.

Reviewing the current mainstream EV isolation strategies, they all have their own advantages and disadvantages. Differential centrifugation and ultrafiltration can process large amount of EV samples at one time, but require long time and much labor, also cannot gain pure EV. SEC and microfluidic methods perform better in EV purity, however, are limited at input volume. Precipitation strategy is popular among many commercialized kits. The precipitation protocol is short, simple and straight-forward. Also, the processing volume of precipitation method can easily serve most of the lab researches. However, the coprecipitation of non-EV molecules and polymer contamination would be the major challenges. Immunoaffinity interaction, or in most of

the cases, immunoprecipitation, is scoring the best in EV separation purity. By choosing antibody for EV surface marker, immunoaffinity method can specifically isolation the EV population of interest. At present, there are commercialized kits, making use of micro magnetic beads with antibody conjugated on the surface, to isolate EVs by targeting the surface markers on the EV membrane. Nevertheless, the prices for antibodies and other reagents can be very high. And the whole procedure generally takes more than 16 hours due to the multiple steps of incubation and washing. Another downside of immunoaffinity purification is that it heavily relies on the chosen marker to isolate target analyte. The expression level or the popularity of the marker can greatly influence the harvested EV population. As a result, the current EV research field is in great need for an isolation strategy with high specificity and purity, simultaneously maintaining large processing volume and fast processing speed. In this project, we propose a binary reagent system, comprising temperature-responsive magnetic nanoparticles and temperature-responsive conjugates to isolate EV via magnetic separation rapidly.

# Chapter 2. TEMPERATURE RESPONSIVE CONJUGATE SYNTHESIS AND CHARACTERIZATION

## 2.1 INTRODUCTION

Smart polymer is a category of polymers which can make responses at the presence of certain stimulus, such as the changes of temperature, pH, humidity, light, specific ions or molecules, electrical fields, solvent and ionic strength etc.[16] Among all the smart polymers, the ones can respond to temperature changes are well-studied because the stimulus change is simple and controllable. For example, poly(N-isopropylacrylamide), or pNIPAAm, known for its sharp and reversible response to physical or chemical stimuli, has been utilized in various biological application such as cell culturing and drug delivery.[17, 18] The temperature-responsive polymer pNIPAAm, as one of the smart polymers, shows a specific hydrophilic-hydrophobic transition when the temperature is above its lower critical solution temperature (LCST), which is about 32 °C. The LCST of pNIPAAm can be controlled by salinity, pH and temperature, making pNIPAAm a convenient smart polymer which can transit its state to serve research purpose simply by introducing corresponding stimulus. The behavior of pNIPAAm from hydrophipic to hydrophobic is due to the conformation change from an expanded, hydrophilic state to a collapsed, hydrophobic state due to the competence of inter- and intra- molecular hydrogen bonding of the pNIPAAm compared to its solubilization by water. [17, 19] When temperature is lower than the LCST, the water molecules in the solution solvate the amide group in pNIPAAm, leading to the formation of structured hydrations shell, thus making the pNIPAAm soluble. However, when the temperature is raised above the LCST, the hydrogen bonding in the hydration shell is weakened, while the hydrophobic interaction from the alkyl groups on the

polymer trunk becomes dominant, which causes the release the water molecules from the pNIPAAm structure. At the same time, the abrupt collapse of polymer chains happens leading to the occurrence of volume phase transition.[16, 20]

So far, the phase transition property of smart polymer pNIPAAm has been utilized in various field such as drug delivery and biomolecule separation. For example, the hydrogel composed of poly(2-hydroxyethyl methacrylate-co-N-isopropylacrylamide)(poly(HEMA-co-NIPAAm)) had been characterized to deliver chlorhexidine diacetate by elevating the temperature from below to above the LCST.[21] The rapid release of antimicrobial drug in this study promised the potential of smart polymer to be utilized as wound dressing or medical devices coatings. Other than drug delivery, there are also researches use pNIPAAm to coat nanoparticles for protein absorption. Shamin *et al* found the pNIPAAm-coated magnetic nanoparticles can absorb and desorb BSA through the polymer phase transition.[22] Principally, the adsorption of BSA was attributed to hydrophobic interaction above the LCST while using pNIPAAm magnetic nanoparticles and hydrogen bonding while using Poly(N-isopropylacrylamide-co-methacrylic acid)(pNIPAAm-MAA) magnetic nanoparticles.

In our previous work, we have introduced the binary reagent system, consisting of a temperature-responsive polymer-antibody conjugate and a temperature responsive magnetic nanoparticle (mNPs).[23] By conjugating multiple temperature-responsive polymers onto an antibody, the resulting conjugate can recognize specific protein target in biological samples and become temperature-responsive simultaneously. Similarly, the magnetic nanoparticles are coated with

temperature-responsive copolymer.[24] The introduction of stimuli, for example, increasing the temperature to 40°C, can result in an aggregation of conjugate-target complex and mNPs, which is separated by magnetic field later. Comparing to existing commercialized microbeads technology, the binary reagent system enables better EV isolation mainly due to three reasons. First, both conjugates and mNPs in binary reagent system exhibit large surface/volume ratio and diffuse rapidly (similar to proteins), which extensively shorten the incubation time before separation. Second, the system can independently increase the amount of applied antibody without increasing mNP to drive the binding kinetics and efficiency. The amount of applied antibody is not limited by mNPs since the conjugate is not covalently linked to the particles. Third, the system can enable rapid magnetic separation by aggregating mNPs and conjugate as big magnetic complexes with high magnetophoretic mobility. The captured target can be separated by magnet within 5 minutes. As a result, the temperature-responsive binary reagent system is used in this project to realize rapid and specific placental EV separation.

## 2.2 MATERIALS AND METHODS

### 2.2.1 *Materials*

N-Isopropylacrylamide ≥99%, Dichloromethane. anhydrous, ≥99.8%, N-Hydroxysuccinimide 0.98, N, N′-Dicyclohexylcarbodiimide, 2,3,5,6-tetrafluorophenyl, N, N′-Diisopropylcarbodiimide, 99%, chloroform ≥99.5% were purchased from Sigma-Aldrich. Hexanes (Certified ACS), 1,4-Dioxane (Certified ACS), Pentane (Certified ACS),

Tetrahydrofuran (Certified) were purchased from Fisher Chemicals. LDS loading buffer and running buffer (novex, NuPAGE) for SDS-PAGE were purchased from Thermo fisher. GelCode™ Blue Stain Reagent was purchased from Thermo scientific. The cell and 4-15% gradient precast gel (PROTEAN series) were purchased from BIORAD. The AffiniPure Goat Anti-Mouse IgG (Fc fragment specific), AffiniPure Goat Anti-Human IgG (Fc fragment specific), AffiniPure Goat Anti-Rabbit IgG (Fc fragment specific), Alexa Fluor® 488 ChromPure Mouse IgG (whole molecule) were purchased from Jackson ImmunoResearch. Sodium Chloride, Potassium Chloride (EMD Chemicals), Sodium Phosphate Dibasic Anhydrous (Granular or Powder/Certified ACS), Potassium Phosphate Dibasic Anhydrous (Crystalline Powder/USP), Sodium Phosphate Monobasic Monohydrate (Crystalline/Certified ACS) were purchased from Fisher Chemicals. Boric Acid, Granular, BAKER ANALYZED™ ACS Reagent Grade and Sodium Borate (10-Hydrate, N.F.) were purchased from J.T.Baker.

### 2.2.2 *Poly (N-isopropylacrylamide) synthesis*

N-isopropylacrylamide should be recrystallized before polymerization reaction. To recrystallize 50g of N-isopropylacrylamide (NIPAAm), firstly add the NIPAAm into 1L hexane in a beaker. Cover the beaker. Slowly heat and stir the solution using a stir bar and hotplate until all NIPAAm is dissolved. Remove the hotplate and cool down the solution to room temperature. Wait for the recrystallization of the NIPAAm. Then, decant the hexane. Cover the beaker with paper towel and dry out the NIPAAm in vacuum chamber.

Poly (N-isopropylacrylamide) is synthesized via reverse addition-fragmentation chain transfer (RAFT). 8g NIPAAm is polymerized by following the recipe (supplemental figure 2.2.2) and the protocol below. Weigh enough N-isopropylacrylamide (NIPAAm) in a beaker. Add 8ml 1, 4-Dioxane to dissolve the NIPAAm. Weigh enough 4-Cyano-4-[(dodecylsulfanylthiocarbonyl)sulfanyl]pentanoic acid (CTA) and 4,4'-Azobis(4-cyanovaleric acid) (Initiator), then add them into the beaker and mix well. Pour the solution into a 25ml or 50ml round bottom flask. Add 2ml Dioxane into the beaker to rinse the beaker, pour the solution into the round bottom flask. Seal the round bottom flask with rubber septum and parafilm (Bemis). Immerse the sealed flask into warm water (around 50°C). Purge the solution by nitrogen for 20 minutes. During the purging, make sure the nitrogen flow does not stop. Redo the purging if the needle is clogged. Plug out the needle after nitrogen purge. Heat the solution at 70°C in oil bath for 4 hours. Stop the polymerization by introducing oxygen (put in a needle or open the seal) and cool down to room temperature. Then, the polymer is precipitated by two protocols according to the synthesis scale.

Pentane precipitation (small scale, 50ml falcon tube protocol): Dilute the polymerization product with Tetrahydrofuran or Dichloromethane or Dioxane to 5~20X volume in a large beaker. Prepare 50ml falcon tubes for precipitation. Add 45ml pentane into each falcon tube. Pipet the diluted polymer solution into the falcon tube slowly (add the polymer drop by drop to make sure complete precipitation). Briefly centrifuge the falcon tubes for 30 seconds at 3000rpm to spin down the precipitated polymer (Beckman GS-6R Benchtop Refrigerated Centrifuge, Marshall Scientific). Discard the supernatant after centrifugation. Repeat the precipitation step until all

polymer solution is precipitated. Do not use caps but paper towel or Kimwipe to seal the falcon tubes. Put the tubes in vacuum chamber for 24 hours to dry out the polymer.

Pentane precipitation (large scale, 1L beaker protocol): Dilute the polymerization product with Tetrahydrofuran or Dichloromethane or Dioxane to 5~20X volume in a large beaker. After mixing well, transfer the polymer solution into a glass funnel. Prepare a 1L beaker for polymer precipitation. Add 25X volume of pentane into the 1L beaker. Hang the glass funnel with polymer solution above the beaker with pentane, use glass plug to control the polymer solution flow. Use a stir bar to stir the pentane while polymer solution is dropping. After all polymer solution is precipitated, add 10ml solvent to rinse the glass funnel, also precipitated the rinsing solution. Set a ceramic funnel onto a conical flask and connect the flask to the fume hood vacuum channel. Put filter paper into the ceramic funnel. Open the vacuum. Pour all the solution from the pentane beaker into the ceramic funnel slowly. Leave the vacuum on for 15 minutes to dry out the precipitated polymer. Scrap off the dry polymer from the ceramic funnel to another glass container. Apply vacuum to the polymer for 24 hours to completely dry out the polymer.

### 2.2.3 *pNIPAAm-antibody conjugate synthesis*

Before the conjugation of pNIPAAm-antibody conjugate, the end-carboxylate of pNIPAAm is activated in order to achieve higher conjugation efficiency.

The end-carboxyl activation of pNIPAAm by N-Hydroxysuccinimide (NHS) is conducted by following the recipe (supplemental figure 2.2.3.1) and protocol below. Dissolve the polymer in anhydrous dichloromethane (DCM) in 25mL round bottom flask. Put a stir bar to help dissolving. Add N, N'-Dicyclohexylcarbodiimide (DCC) and N-Hydroxysuccinimide (NHS) after the polymer is dissolved. Stir overnight in fume hood under room temperature. Take out the stir bar, attach the flask to the rotavapor (Büchi R-124 Rotary Vap System, Büchi). Adjust the vacuum flow to assure small bubbling in the flask. Set the flask rotation speed at 75-120rpm, rotate for 40-60 minutes until the solution become dry. Attach the flask to the vacuum pump for 12 hours for further dry out.

The end-carboxyl activation of pNIPAAm by Tetrafluorophenyl (TFP) is conducted by following the recipe (supplemental figure 2.2.3.2) and protocol below. Dissolve the 1g polymer in 5mL DCM in a 25mL round bottom flask. Put a stir bar to help dissolving. Add 46.1mg Tetrafluorophenyl (TFP) and 278uL N, N'-Diisopropylcarbodiimide (DIC) solution after the polymer is dissolved. Stir overnight in fume hood under room temperature. Take out the stir bar, attach the flask to the rotavapor. Adjust the vacuum flow to assure small bubbling in the flask. Set the flask rotation speed at 75-120rpm, rotate for 40-60 minutes until the solution become dry. Attach the flask to the vacuum pump for 12 hours to further dry out.

A small-scale conjugation tryout is conducted before large-scale conjugation. 4 pNIPAAm/antibody ratios (25:1. 50:1, 100:1, 200:1) are tested to find out the optimal conjugation ratio. An anti-mouse IgG conjugate tryout is planned by following the protocol.

Mix the reagents in 2.0mL tube according to the table (Supplemental figure 2.2.3.3, Supplemental figure 2.2.3.4). Vortex to dissolve the polymer in solution. During the dissolving of polymer, make sure the solution does not generate too much heat. Use parafilm to seal the tubes. Set the tubes in rotator in 4°C overnight.

Large scale conjugation using 200:1 polymer/antibody ratio apply the same protocol. (Supplemental figure 2.2.3.5) After the overnight incubation of conjugation, the unconjugated antibody should be removed before SEC purification. All tubes are water-bathed at 40°C for 10 minutes. Centrifuged at 12000 rpm for 5 minutes at 40°C (Refrigerated Centrifuge 5418 R, Eppendorf). Collect the supernatant immediately for antibody recycling. Add 500uL PBS to resuspend the conjugate and polymer. 4°C incubate overnight.

The resulting conjugate solution is further purified through Size Exclusion Chromatography (SEC). Two different HPLC systems have been used to purify the conjugate.

① BioCAD working station (PerSeptive Biosystems) equipped with Biosep SEC-s4000 column (Phenomenex): Set up the flow rate at 5 ml/min, run time at 23 minutes and UV detector at 280nm. Purge the system before injection. Prepare enough 0.22μm-filtered DI water to rinse injector seat (Barnstead Nanopure Diamond Lab Water System, Thermo Scientific) (Acrodisc® Syringe Filter with Supor® Membrane - GxF/0.2 μm, 25 mm (PALL), syringe and needles. Use 0.22μm filter to filter all conjugate samples. Do one or two water injection (2.5mL) before sample injection, make sure no peak is observed. During conjugate injection (1 mL), collect the flow-out manually when antibody peak appears. Before switching to different conjugate samples,

run water injection to flush out potential residue in column. After the last sample injection, run one more water injection to wash the column. The mobile phase used in BioCAD system is boric acid buffer (pH 8.0). To make 7.4L boric acid buffer, dissolve 30.525g boric acid in 1.55L deionized water and 9.12g sodium borate 10-Hydrate in 1.2L deionized water. Use sodium borate to titrate the pH to 8.0. Use 0.22μm filter to filter the buffer twice (Steritop Threaded Bottle Top Filter, Sterile, 1000 mL process volume, 0.22 μm pore size, GP, 45 mm, polyethersulfone membrane, EMD Millipore). Use 0.22μm-filtered deionized water to rinse all containers before pouring the buffer into them.

②Agilent-6520 QTOF system (Agilent) equipped with Yarra SEC-s4000 column (Phenomenex): Set up the flow rate at 4.5mL/min. Set up the UV detector to monitor 306nm and 280nm. Set up the run time for each injection at 35 minutes. Mobile phase used in Agilent-6520 QTOF system is 0.1M sodium phosphate buffer (pH 6.8). To prepare 1 L 0.1M sodium phosphate buffer (pH 6.8), firstly add 800 mL of DI water in a container, then weigh 13.124 g of $Na_2HPO_4$-$7H_2O$ and 7.043 g of $NaH_2PO_4H_2O$ and add them into the DI water. Adjust solution to final desired pH using HCl or NaOH and add DI water until volume is 1 L. During the first conjugate injection, collect the direct column flow out fractions for every 30 seconds, measure the UV absorbance of 280nm and 306nm in another UV-vis spectrophotometer (Hewlett-Packard - HP 8452A Diode Array Spectrophotometer, Agilent Technologies). Compare the UV spectrums to the chromatograms shown on the Agilent System, calculate the delay between the UV signal and direct flow out.

After SEC-purified conjugate was collected, they need to go through Amicon concentration to concentrate the conjugate and further removing small impurities (Amicon® Ultra-15 Centrifugal Filter Unit, Merck Millipore). Before using Amicon Ultra-15 100K centrifugal unit, add 15ml PBS buffer (pH 7.4) into the tube and apply 5-minute centrifugation at 2740rpm to wash the membrane. Add collected conjugate solution into Amicon tube, centrifuge at 2740 rpm for 10 minutes. Discard to the flow-through. Repeat until all conjugate solution is concentrated. At the end, add 200uL PBS to rinse the membrane, combine it with the concentrate. Use UV-vis spectrophotometer to measure the concentration of conjugate.

Use Amicon Ultracel-3k for antibody recycling after thermal precipitation. Add 15ml PBS buffer into Amicon tube, 3700rpm centrifuge for 15 minutes to rinse the membrane. Discard the flow-through. Add the supernatant from thermal precipitation into the Amicon tube, add PBS buffer to dilute it to 15mL. Centrifuge 30 minutes at 3700rpm. Discard the flow-through. Add PBS buffer into the tube to dilute the concentrate to 15mL. Repeat the centrifugation twice. Collect the concentrate in the membrane. Measure the protein concentration by UV-vis spectrophotometer. UV-vis spectrophotometer is used to estimate the antibody concentration of the purified conjugate and recycled antibody. Since every conjugate consists of one antibody and multiple polymers, to facilitate the calculation, the conjugate concentration is expressed by the antibody concentration. The antibody concentration is calculated according to Beer's Law: $A = \varepsilon Lc$. By rearranging the law to solve the sample concentration, we have: $c=A/\varepsilon L$, in which c is the molar concentration of the sample, A is the amount of light absorbed by the sample for a particular wavelength, $\varepsilon$ is the molar extinction coefficient, L is the distance that the light travels through the solution. In this equation, A is shown as Actual Absorbance on the UV-vis

spectrophotometer, L is 1 cm, ε is 210,000M-1 cm-1 for all the antibodies being used in the project. Typically, conjugate has two absorption peaks at 280nm and 307nm indicating antibody and polymer respectively. By assuming each peak has a symmetric profile, the real antibody absorbance at 280nm equal to the absorbance at 280nm minus absorbance at 334nm (307nm+(307nm-280nm)).

### 2.2.4 *Synthesizing and characterizing magnetic nanoparticles*

The synthesis and characterization of magnetic nanoparticles (mNPs) used in the study was reported in the previous work. [24] In brief, the mNPs was synthesized via an in-situ co-precipitation process of iron cation salts with a diblock co-polymer poly (acrylic acid)-block-poly(N-isopropylacrylamide) by RAFT. The resulting magnetic nanoparticles apply a 6.5:1 Fe/COOH ratio and are 56% polymer by weight. In a 2-month span, the synthesized mNPs are very stable, with hydrodynamic diameter staying constant at around 28nm, transition temperature staying at 34°C and maintaining separation efficiency over 95% while applying 40°C magnetic separation protocol. The synthesis of mNPs by our protocol is reproducible, and the functions of mNPs are stable across different batches.

### 2.2.5 *$^{1}$H NMR characterization*

The $^{1}$H NMR spectra of synthesized pNIPAAm were obtained in $CDCl_3$ on Bruker Avance spectrometer at 300 MHz, installed with the probe: PABBI: X(1H) as - multi nuclear. While preparing the sample, dissolve the lyophilized polymer (FreeZone Plus 4.5 Liter Benchtop

Freeze Dryer, Labconco), in 600uL chloroform-d. Follow the standard protocol to operate the system.

### 2.2.6 *GPC characterization*

The molecular weight and polydispersity of the synthesized pNIPAAm were characterized by the gel permeation chromatography (GPC). GPC was performed on Agilent 1200 series with two TSKgel Alpha-3000 and one TSKgel Alpha-4000 in series at 60°C, a mini DAWN TREOS three angle light scattering detector and an Optilab T-rEX refractive index detector. The mobile phase was HPLC-grade DMF (0.1% lithium bromide) at 1 mL/min. The lyophilized pNIPAAm was dissolved in dimethylformamide (DMF) at a concentration of 5mg/mL. And the resulting samples would be 0.22μm-filtered before the injection to prevent potential clogging in the column.

### 2.2.7 *SDS-Polyacrylamide Gel Electrophoresis*

According to the solution volume, add 4X LDS loading buffer into each tube of conjugate. Prepare one more sample with equal amount of anti-mouse IgG as a control. Set all tubes in a thermo cycler. Thermo cycling is programmed to process all samples before loading onto gel (Perkin-Elmer/ Cetus DNA Thermal Cycler, Perkin Elmer). (Supplemental figure 2.2.7) Use gel-loading tips to load 20uL of sample in each well on a Biorad 4-15% gradient gel. Apply 150V constant voltage for 45 minutes (FisherBiotech FB400 electrophoresis system, Fisher Scientific). Take out the gel and use DI water to rinse the gel for 30 minutes on a shaker (Model55 rocking

shaker, MIDSCI), then decan the water. Add Gel-Code blue staining reagents to stain the gel on the shaker for 45 minutes. Decan the staining reagents and add DI water to destain on the shaker overnight.

### 2.2.8 *Target binding characterization of polymer-antibody conjugates*

In order to investigate the optimal conjugate/target ratio for separation, 5 conjugate/target ratios (1:10, 1:3.3, 1:1, 3.3:1, 10:1) are tested. A binding titration for anti-mouse IgG conjugate is planned as the following table (Supplemental figure 2.2.8.1~ 2.2.8.3). In a binding titration experiment, fixed amount of fluorescent mouse IgG are mixed with different amount of anti-mouse IgG conjugates according to the designed conjugate/target molar ratio. Then the mNPs and salt are added into the solution. In this step, adding additional sodium chloride can lower the LCST of mNPs, which will make the magnetic separation sharper at 40°C. Gently vortex and quickly spin down the solution (Fisher Scientific Vortex Mixer, Fisher brand)(Corning® LSE™ Mini Microcentrifuge, Corning). Set the tubes in 40°C water bath for 5 minutes (General Purpose Water Baths Model 182, PRECISION). Move the tubes onto a magnetic rack to perform magnetic separation for 5 minutes. Collect the supernatant carefully. Pipet 200uL supernatant in each group onto a 96-well plate for fluorescent measurement. The concentrations of fluorescent mouse IgG in each supernatant fraction are back calculated by fluorescent standard curve. A 5-minute water bath at 40°C can aggregate the target-conjugate complex and mNPs together. Subsequently, all the tubes are transferred to rack with a magnet immobilized at one side to attract the target-conjugate-mNPs aggregates. 200uL of the supernatant is collected from each tube and is analyzed by fluorescence plate reader (The Infinite® M1000 plate reader, Tecan).

## 2.3 Results and Discussion

### 2.3.1 *Polymer characterization*

Scheme 1: RAFT-mediated polymerization of NIPAAm.

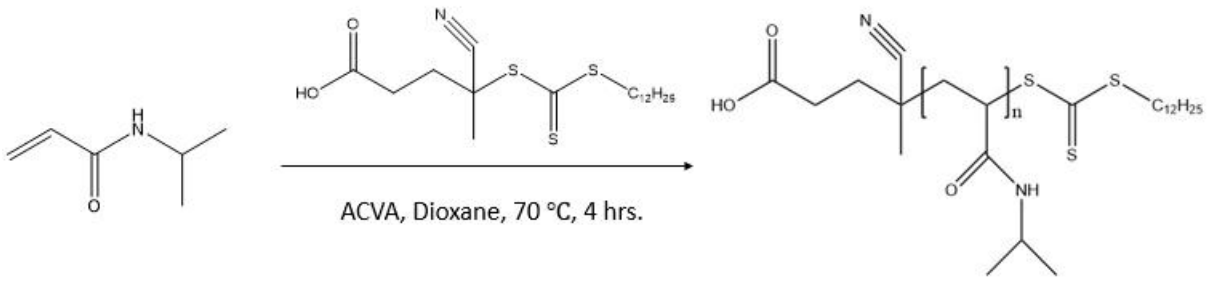


Scheme 1 illustrate the synthesis of poly(N-isopropylacylamide) (pNIPAAm) via reverse addition-fragmentation transfer (RAFT) with the presence of a chain transfer agent (CTA) and a radical source (initiator). RAFT is a polymerization method to provide good molecular weight control and narrow molecular weight distribution. It can be performed readily as a classical free radical polymerization with an addition of a thiocarbonylthio compound. RAFT is a versatile polymerization method to polymerize most of the vinyl monomers and accommodate various solvent system. Compared to conventional free radical polymerization method, RAFT allows for preparing polymer with well-defined architecture, such as graft, block, comb, star and brush. By synthesizing pNIPAAm via RAFT, every polymer chain had a carboxylate group provided by

CTA, which could be transformed to active ester for downstream polymer-antibody conjugate synthesis. Also, the pNIPAAm synthesized via RAFT had a narrow molecular weight distribution, which could control the polymer's transition temperature precisely. The pNIPAAm synthesis utilized 4-Cyano-4-[(dodecylsulfanylthiocarbonyl)sulfanyl]pentanoic acid as the CTA because the resulting polymer will exhibit a end carboxylate to enable the antibody conjugation. The polymer synthesis targeted 400 degree of polymerization (DP) with 85% conversion. The polymerization was carried out at 70°C for 4 hours. After the polymerization, the polymer chains were isolated by precipitation, and then characterized using $^{1}$H NMR (Figure 2.3.1.1) and gel permeation chromatography (GPC) for the polymer composition, and molecular weight with the associated polydispersity (Figure 2.3.1.2).

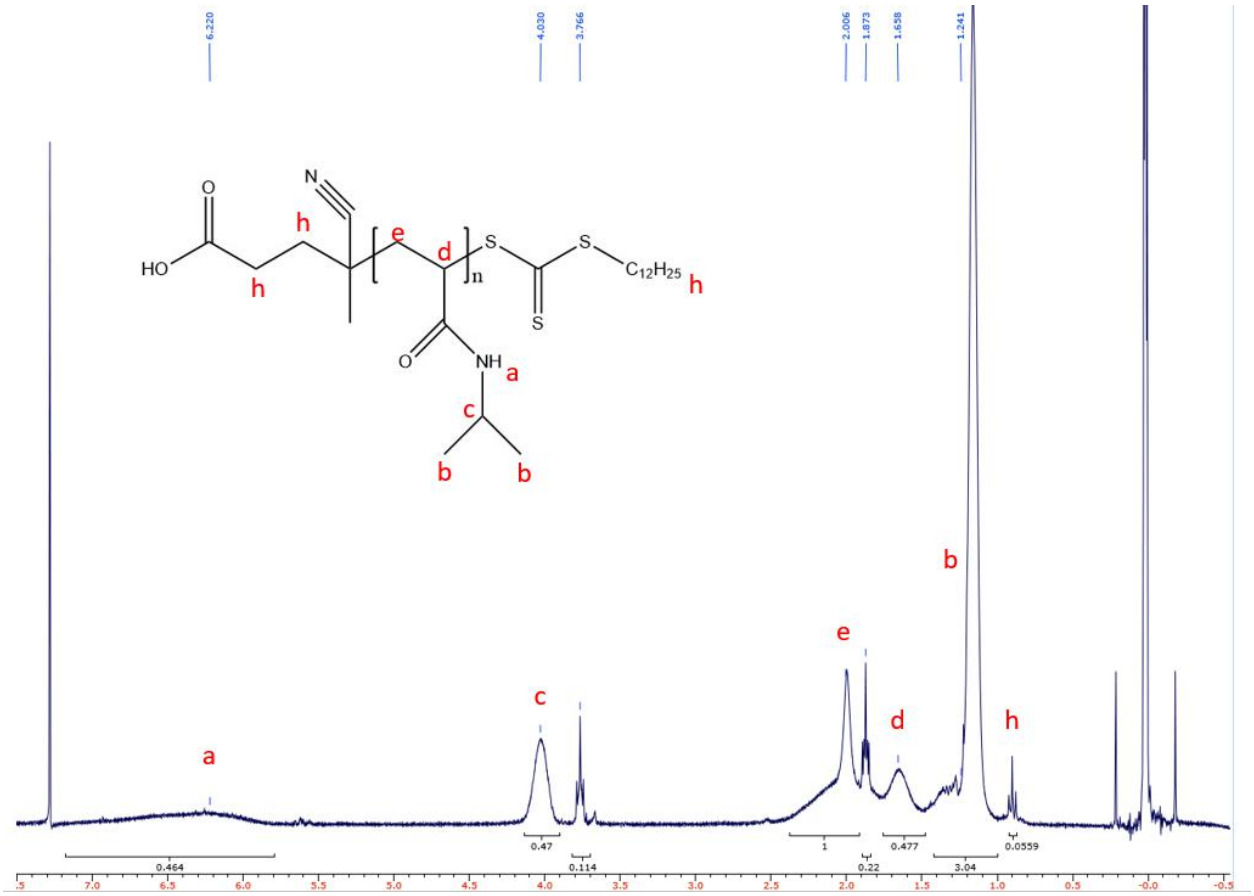


Figure 2.3.1.1: $^{1}$H NMR spectroscopy of pNIPAAm.

The peak at 6.22 ppm in the $^{1}$H NMR spectrum confirmed the presence of the proton on the amide nitrogen atom (N*H*–) of NIPAm repeating units, the peak at 1.24 ppm was attributed to the methyl (C$H_3$–) protons of NIPAm repeating units, the peak at 4.03 ppm belonged to the alkyl proton (C*H*–) near the nitrogen atom, and the alkyl CH and $CH_2$ on the PNIPAm main chain appeared as the peaks at 1.65 and 2.00 ppm, respectively. The peak at 0.9 ppm was attributed to the alkyl protons from CTA. And the two unidentified peaks at 1.87 and 3.76 ppm might result from the small molecule impurities in solution. (Figure 2.3.1.1).

GPC analysis (Figure 2.3.1.2) showed the number average molecular weight ($M_n$) of the synthesized pNIPAAm was 29070, corresponding to 254 monomeric units of NIPAAm with a polydispersity index (PDI) at 1.186. $^1$H NMR analysis (Figure 2.3.1.1), ratio of chemical shift h over chemical shift a, shows ca. 250 average degree of polymerization. The light scattering (LS) signal and differential refractometer (dRI) signal showed identical retention time at 25 minutes. The dRI chromatogram showed only one peak with the retention time at 25 minutes, indicating the purity of polymer solution. The LS chromatogram showed only one peak with a tiny shoulder, indicating a little heterogeneity of molecular weight of the synthesized pNIPAAm.

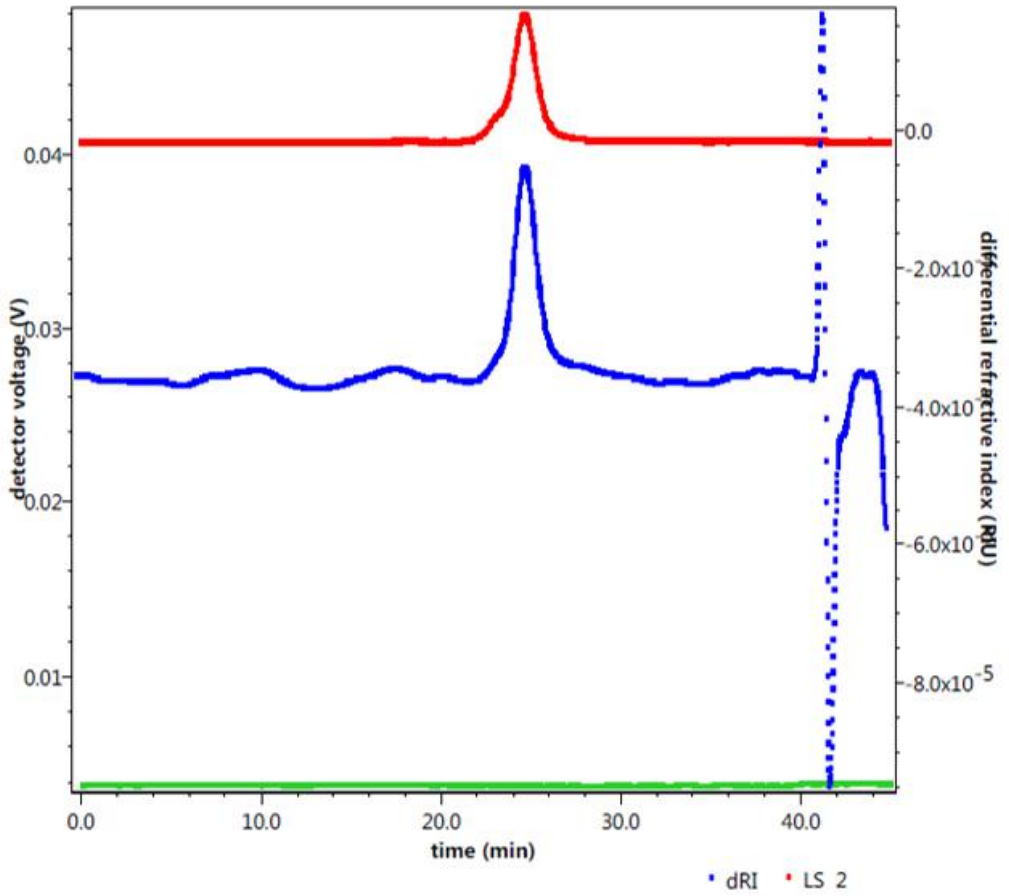

Figure 2.3.1.2: GPC characterization of pNIPAAm.

The light scattering (LS) signal and differential refractometer (dRI) signal were displayed in the figure, both of them showed identical peak at around 25 minutes. The red curve in the figure, which represented the light scattering signal, displayed a tiny shoulder before the peak at around 25 minutes, indicating a small amount of higher molecular weight pNIPAAm with more repeating units. The blue curve, which represented the differential refractometer signal, displayed a peak at an identical retention time as light scattering signal, confirming the purity of the synthesized pNIPAAm.

### 2.3.2 *Synthesizing pNIPAAm-antibody conjugate*

Before the polymer antibody conjugation, the end carboxyl group of pNIPAAm was converted to tetrafluorophenyl (TFP) or N-Hydroxysuccinimide (NHS) ester via carbodiimide chemistry. The activated pNIPAAm was subsequently conjugated to the primary amines on the antibody, immunoglobulin G (IgG), efficiently by forming an amide bond. Aiming for complete conjugation of antibody, excess amount of polymer was used in the reaction. A small-scale tryout for evaluating conjugation efficiency varied the polymer:antibody ratio from 25:1 to 200:1. SDS-PAGE, a common analytical method for protein separation, was used to characterize the resulting conjugates. In the SDS-PAGE gel image (Figure 2.3.2), lane 5 is the native antibody. The polymer/antibody ratio was 25:1 for lane 1/2, was 50:1 for lane 3/4, was 100:1 for lane 6/7 and was 200:1 for lane 8/9. The polymer cannot be stained by Gel Code blue, thus the blue stain in the image only represented either the native antibody or polymer-antibody conjugates. The polyacrylamide gels are restraining the larger molecules from migrating as fast as smaller

molecules. Therefore, the conjugate (larger molecular weight) ends up having a shorter migrating distance compared to antibodies (smaller molecular weight). And with the increasing of polymer/antibody molar ratio, the native antibody band stain intensity was reduced since more antibody were conjugated. The resulting conjugates show no detectable native antibody on SDS-PAGE were considered to be the desired polymer/antibody ratio for larger scale synthesis. Both 25:1 and 50:1 molar ratios showed discrete band with slightly higher molecular weight than native antibody, indicating the presence of conjugates with constant numbers of grafted polymer. The native antibody band disappeared at 200:1 ratio, indicating nearly completion conjugation the antibody with polymer. All conjugations show a clear stain with smear pattern in the loading well, which confirm the successful conjugation with higher molecular weight than native antibody. The smear pattern suggests the resulting conjugates have wide molecular weight distribution, caused by conjugating with varied numbers of polymer on a single antibody.

Every new NHS- or TFP-pNIPAAm was evaluated for its conjugation efficiency by varying polymer:antibody ratio from 50:1 to 400:1. In practice, the details in protocol could make a difference in the conjugation efficiency. For example, keep the tubes in ice bath while mixing the polymer in antibody could prevent excess heat from the friction of vortexing. Also, TFP-pNIPAAm exhibits better conjugation efficiency than NHS-pNIPAAm because better hydrolysis resistance due to its hydrophobicity.

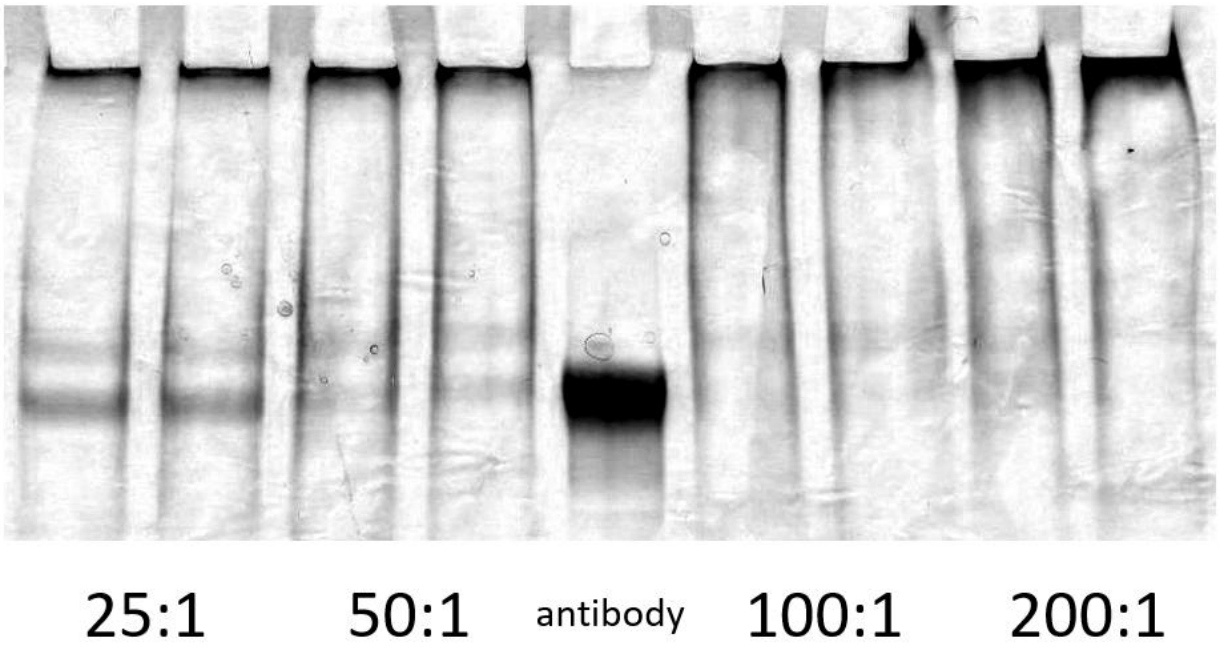


Figure 2.3.2: SDS-PAGE gel of conjugation tryout: Stained SDS-PAGE gel.

Both 25:1 and 50:1 molar ratios showed discrete band with slightly higher molecular weight than native antibody, indicating the presence of conjugates with constant numbers of grafted polymer. The native antibody band disappeared at 200:1 ratio, indicating most of the antibody were conjugated with polymer. All conjugations show a clear stain with smear pattern in the loading well, which confirm the successful conjugation with higher molecular weight than native antibody. The smear pattern suggests the resulting conjugates have wide molecular weight distribution, caused by conjugations in which the varied numbers of polymer are grafted on a single antibody.

The conjugate purification strategy was designed based on the components in conjugate solution. After the conjugation of pNIPAAm and antibody, there were various components in solution, including pNIPAAm-antibody conjugates, unconjugated pNIPAAm, unconjugated antibody and

other impurities from carbodiimide chemistry, even if the large-scale conjugation chose to use a pNIPAAm/antibody ratio which minimized the amount of unconjugated antibody. In total, three steps of purification are used to remove the free antibody, free polymer and concentrating the conjugate. The first thermal-precipitation step was able to remove the unconjugated antibody and the impurities. Thermal-precipitation started with a 5-minute heating at 40°C by water bath, which would aggregate the conjugates and free polymer together. A subsequent thermal centrifugation at 40°C could pellet the aggregates from the solution. The supernatant was always collected in case there was considerable amount of native antibody to be recycled. Then, the pellet would be resuspended in buffer and go through another 24-hour incubation. An SDS-PAGE at this step to confirm all fractions was suggested for quality control. (Supplemental figure 2.3.2.1) The second step is size exclusion chromatography (SEC). Since the size exclusion chromatography can differentiate the molecules according to their hydrodynamic radius, it became an optimal option to separate pNIPAAm-antibody conjugate from excess pNIPAAm. A SEC column is always packed with porous resin, in which the bigger molecules fail to go through most of the pores and will flow out quickly, while the smaller molecules are taking longer time to travel through the pores. Before using SEC for conjugate purification, three standard proteins and a purified polymer-antibody conjugates were injected through the column to confirm the column capacity of separating conjugates from proteins and polymer. The chosen standard samples included insulin (5808 Da), BSA (66kDa), mouse IgG (150kDa), polymer-antibody conjugate (>200kDa), having a retention time of 20 minutes, 17.5 minutes, 16 minutes and 12 minutes, respectively. By overlaying all the chromatograms, every peak is separated from each other, confirming that the column can be used to separate conjugate from antibody and polymer. (Supplemental figure 2.3.2.2)

After the conjugates were resuspended and incubated overnight, they were filtered using 0.22µm syringe filter and aliquoted before injection. The chromatograms for the first conjugate injection were used to analyze the optimal collecting time. The UV signal at 280nm (antibody) and 306nm (polymer) both went up at 11 minutes, reaching the highest at around 13.5 minutes, and then decreased until 16 minutes. The UV signal at 306nm went up again after 16 minutes, which was resulting from the appearance of pNIPAAm. (Figure 2.3.2.2)

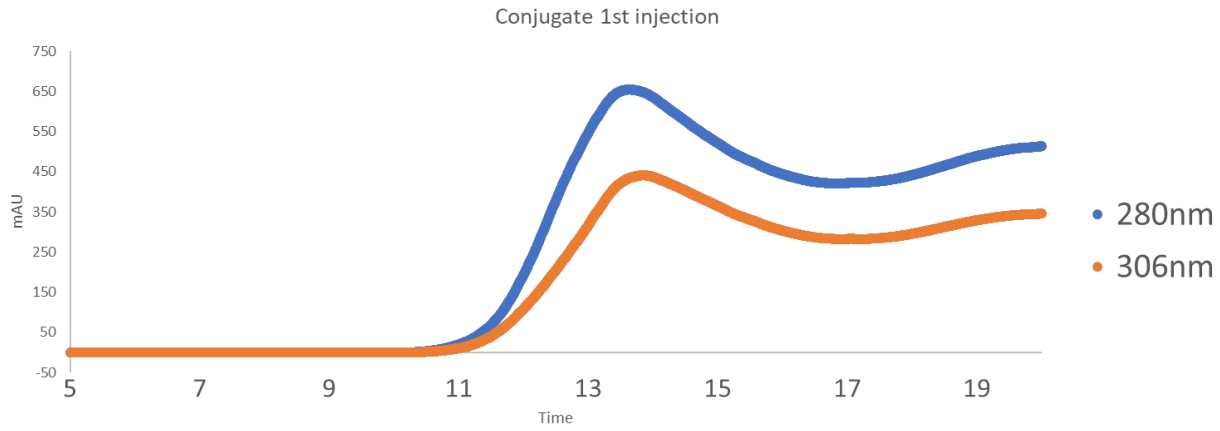


Figure 2.3.2.2: SEC chromatograms of pNIPAAm-antibody conjugates.

The UV signal at 280nm (antibody) and 306nm (polymer) both went up at 11 minutes, reaching the highest at around 13.5 minutes, and then decreased until 16 minutes. The UV signal at 306nm went up again after 16 minutes, which indicated the appearance of pNIPAAm.

Due to the flow rate difference between UV-detector and the direct flow out from the column, all the collected samples from column need to be analyzed again by a benchtop UV-vis

spectrophotometer. For every 30 seconds starting from 6 minutes to 17 minutes, totally 22 fractions were collected and characterized again. (Figure 2.3.2.3) The resulting UV spectrums had similar profile with the SEC chromatograms, but the retention time derived from these UV spectrums were 2 minutes less when comparing to the SEC chromatograms. It was because the flow rate in the SEC detector tubing was too slow, causing an approximately 2 minutes delay between the detector signal and direct flow out from column. To further confirm the collecting time for pure conjugate, the result of 280nm absorbance minus 334nm absorbance for each fraction was calculated and plotted. This calculation was based on the assumption that the profile of UV absorbance peak was symmetrical, so the polymer absorbance at 334nm (280+(307-280) *2) was equal to the polymer absorbance at 280nm. By subtracting polymer absorbance at 280nm from the raw absorbance reading at 280nm, we should get the antibody absorbance at 280nm which represented the conjugate. From the UV spectrums, the conjugate signal, which was shown as 280nm-334nm, started at 8.75 minutes and ended at 13.25 minutes, which was confirmed as the conjugate collection time.

Since the collected conjugate from SEC column is extensively diluted compared to which before the injection, the last step of purification is to use Amicon centrifugal unit to concentrate the conjugate. The Amicon centrifugation unit being used have a molecular weight cutoff at 100,000 or 50,000. Upon the centrifugation, the molecules with a molecular weight larger than the cutoff will be retained in the membrane while the small molecules will go through the membrane. At last, UV-vis spectrophotometer is used to measure the concentration of the purified and concentrated conjugate.

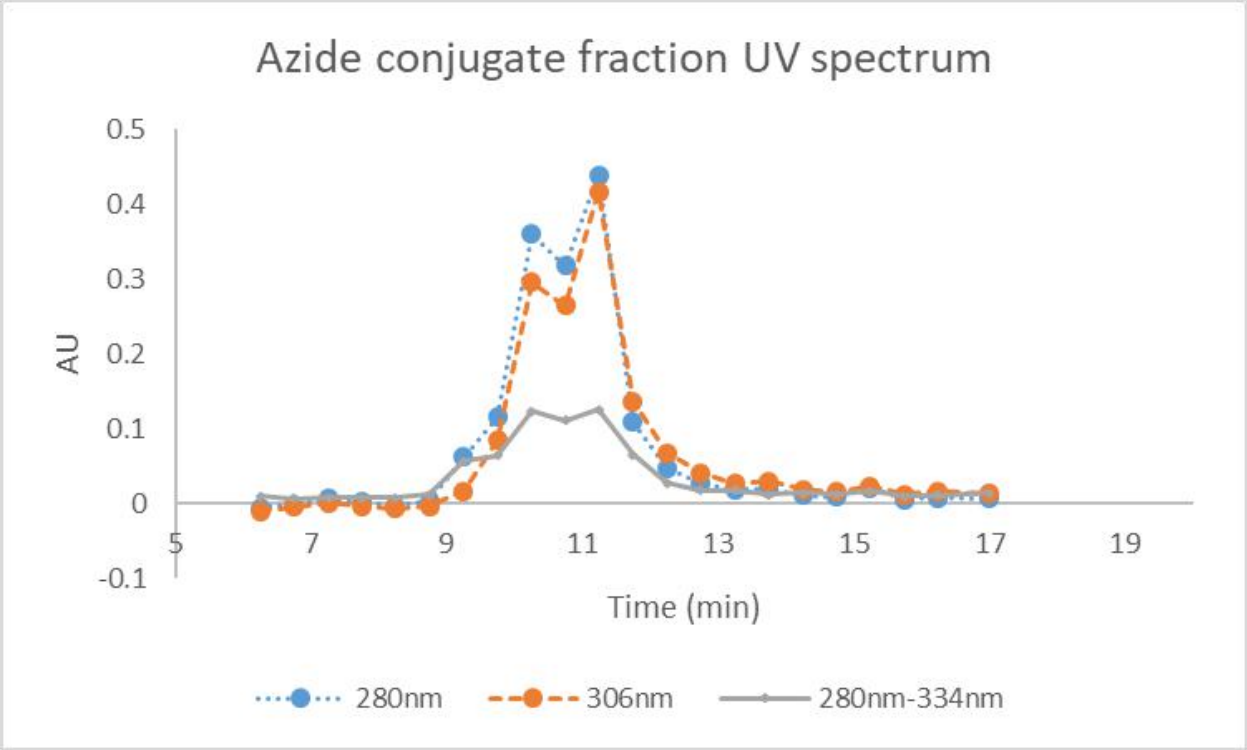


Figure 2.3.2.3: UV-vis spectrums of collected fractions from SEC.

The UV spectrums had similar profile with the SEC chromatograms, but the retention time derived from these UV spectrums were 2 minutes less when comparing to the SEC chromatograms, indicating a 2-minute delay between the SEC detector signals and direct flow out from column. The conjugate signal, which was shown as 280nm-334nm, started at 8.75 minutes and ended at 13.25 minutes, which was confirmed as the conjugate collection time

### 2.3.3 *Binding titration of polymer-antibody conjugate*

The capture efficiency of purified conjugates was characterized by titrating constant amount of target analytes with various molar ratios of conjugates. For example, Figure 2.3.3 showed the binding titration for 6 batches of anti-mouse IgG conjugates. The target analyte is 0.11μM Alexa

Fluor® 488 labeled mouse IgG, 5μg mouse IgG in 300μl final volume. The conjugate:mouse IgG molar ratio varies from 0.1:1 to 10:1. Because the mouse IgG is labeled with Alexa Fluor 488, the separation efficiency can be quantitated by normalizing the solution fluorescent intensity after the separation to the standards of Alexa Fluor 488 labeled mouse IgG standards. When the conjugate/mouse IgG ratio was lower than 1:1, the estimated separation efficiency was less than 20% after the separation. When the conjugate/mouse IgG ratio was 1:1, the estimated separation efficiency was 42±3.7% after the separation. When the conjugate/mouse IgG ratio was 3.3:1, the estimated separation efficiency increased to 81.4±5.2% after the separation. The separation efficiency increased further when the conjugate:mouse IgG ratio was further increased. The separation efficiency reached 91.4%±2.2% when the conjugate:mouse IgG raito was 10:1 and did not further increase for higher conjugate:mouse IgG ratio, which suggests that the separation was near maximum. The remaining solution fluorescent signal is likely caused by the denatured mouse IgG and/or free Alexa Fluor 488.

Different conjugate batches require different conjugate/target ratio to achieve maximum separation, ranging from 3.3:1 to 15:1. The variation might be caused by different antibodies that were used for the conjugate synthesis, errors associated with the estimations for the conjugate concentration, and target analytes (e.g., fluorescent protein).

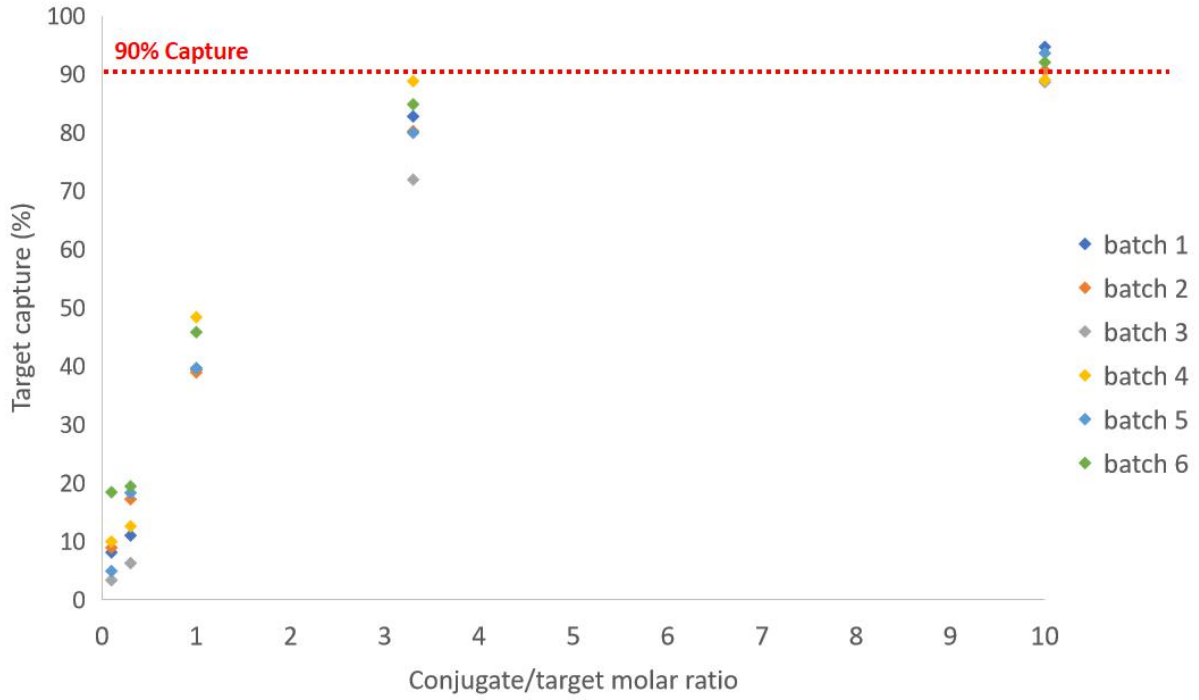


Figure 2.3.3: Binding titration of 6 batches anti-mouse IgG conjugates.

When the conjugate/mouse IgG ratio was lower than 1:1, the estimated separation efficiency was less than 20% after the separation. The separation efficiency increased further when the conjugate:mouse IgG ratio was further increased. The separation efficiency reached 91.4%±2.2% when the conjugate:mouse IgG raito was 10:1 and did not further increase for higher conjugate:mouse IgG ratio, which suggests that the separation was near maximum.

Fluorescent measurement settings: emission: 495nm, excitation: 525nm, plate reader gain: 80.

## 2.4 CONCLUSION

In the study, the temperature-responsive poly(N-isopropylacrylamide) was synthesized via RAFT polymerization. $^{1}H$ NMR confirmed the composition of pNIPAAm and GPC characterization showed the number average molecular weight (Mn) of the synthesized pNIPAAm was 29070 with a polydispersity index (PDI) at 1.186. The pNIPAAm was then modified by NHS or TFP via carbodiimide chemistry. The modification started from a small-scale tryout of pNIPAAm and antibody conjugation which investigated multiple polymer/antibody ratio for conjugations. The SDS-PAGE analysis of the tryout discovered a polymer/antibody ratio of 200:1 was the optimal ratio among all TFP-pNIPAAm antibody conjugations. The scalable synthesis following the optimal polymer/antibody ratio was done subsequently. The conjugate went through thermal-precipitation, SEC purification and Amicon concentration to remove impurities and excess polymer. A binding titration which investigated a series of conjugate/target molar ratio was conducted to characterize the binding capacity of conjugate using fluorescent target protein (fluorescent mouse IgG). For most of the conjugates, a conjugate/target ratio at 10:1 could achieve over 90% of target capture.

## 2.5 SUPPLEMENTAL INFORMATION

Supplemental figure 2.2.2: NIPAAm polymerization via RAFT

| | F.W. | Molar | Weight | Volume |
|---|---|---|---|---|

| | | ratio | | |
|---|---|---|---|---|
| N-isopropylacylamide | 113 | 400 | 8.062g | |
| 4-Cyano-4-[(dodecylsulfanylthiocarbonyl)sulfanyl]pentanoic acid (Chain transfer agent) | 403.67 | 1 | 0.072g | |
| V-501 (Initiator) | 280.28 | 0.1 | 0.005g | |
| Dioxane | | | | 10 ml |

Supplemental figure 2.2.3.1: pNIPAAm end carboxyl activation by NHS

| Reagents | F.W. | Mass (g) | Volume (mL) | Molar ratio |
|---|---|---|---|---|
| pNIPAAm | 36,000 | 1.5 | | 1 |
| Dichloromethane (anhydrous) | | | 18 | |
| N, N′-Dicyclohexylcarbodiimide (DCC) | 206 | 0.188 | | 22 |
| N-Hydroxysuccinimide (NHS) | 115 | 0.092 | | 20 |

Supplemental figure 2.2.3.2: pNIPAAm end carboxyl activation by TFP

| Reagents | F.W. | Mass (g) | Volume (mL) | Mole | Molar ratio |
|---|---|---|---|---|---|
| pNIPAAm | 36,000 | 1 | | 0.0000278 | 1 |
| Dichloromethane (anhydrous) | | | 5 | | |
| N,N'-Diisopropylcarbodiimide (DIC) | | | 0.278 | 0.000278 | 10 |
| Tetrafluorophenyl (TFP) | 166 | 0.046 | | 0.000278 | 10 |

Supplemental figure 2.2.3.3: Reagents for NHS-pNIPAAm and antibody conjugation.

| Reagents | Concentration |
|---|---|
| Anti-mouse IgG | 0.5mg/ml |
| NHS-pNIPAAm (dissolved in anhydrous DMSO) | 276mg/ml |
| Sodium bicarbonate | 2 M |

Supplemental figure 2.2.3.4: NHS-pNIPAAm antibody conjugation tryout

| pNIPAAm/antibody molar ratio | NHS-pNIPAAm (uL) | Anti-mouse IgG (uL) | Sodium bicarbonate (uL) | Total (uL) |
|---|---|---|---|---|
| 25:1 | 0.5 | 46 | 3.5 | 50 |
| 50:1 | 1 | 46 | 3 | 50 |
| 100:1 | 2 | 46 | 2 | 50 |
| 200:1 | 4 | 46 | 0 | 50 |

Supplemental figure 2.2.3.5: NHS-pNIPAAm antibody conjugation with 200:1 ratio in large scale

| pNIPAAm/antibody molar ratio | NHS-pNIPAAm (uL) | Anti-mouse IgG (uL) | Sodium bicarbonate (uL) | Total (uL) |
|---|---|---|---|---|
| 200:1 | 180 | 1600 | 0 | 1800 |

Supplemental figure 2.2.7: Thermo-cycler program for sample preparation

| Stage | Temperature (°C) | Time (minute) |
|---|---|---|
| 1 | 95 | 0.5 |
| 2 | 95 | 4.5 |

| | | |
|---|---|---|
| 3 | 25 | Hold |

Supplemental figure 2.2.8.1: Reagents for binding titration of anti-mouse IgG conjugate

| Reagents | Concentration |
|---|---|
| Fluorescent mouse IgG (f-mIgG) | 1mg/ml |
| Anti-mouse IgG conjugate (conjugate) | 1mg/ml |
| Sodium chloride (NaCl) | 2 M |
| Magnetic nanoparticles (mNP) | 10 mg/ml |

Supplemental figure 2.2.8.2: Binding titration of anti-mouse IgG conjugate

| # | f-mIgG (uL) | Conjugate (uL) | Conjugate/target molar ratio | PBS (uL) | NaCl (uL) | mNP (uL) | Total (uL) |
|---|---|---|---|---|---|---|---|
| 0 | 5 | 0 | 0 | 235 | 30 | 30 | 300 |
| 1 | 5 | 0.5 | 1:10 | 234.5 | 30 | 30 | 300 |
| 2 | 5 | 1.65 | 1:3.3 | 233.35 | 30 | 30 | 300 |
| 3 | 5 | 5 | 1:1 | 230 | 30 | 30 | 300 |
| 4 | 5 | 16.5 | 3.3:1 | 218.5 | 30 | 30 | 300 |
| 5 | 5 | 50 | 10:1 | 185 | 30 | 30 | 300 |

Supplemental figure 2.2.8.3: Fluorescent standard curve

| # | f-mIgG (uL) | PBS (uL) | Total (uL) |
|---|---|---|---|
| F1 | 5 | 295 | 300 |
| F2 | 2.5 | 297.5 | 300 |
| F3 | 1.25 | 298.75 | 300 |
| F4 | 0.625 | 299.375 | 300 |
| F5 | 0.3125 | 299.6875 | 300 |

Supplemental figure 2.3.2: Image J analysis of SDS-PAGE gel.

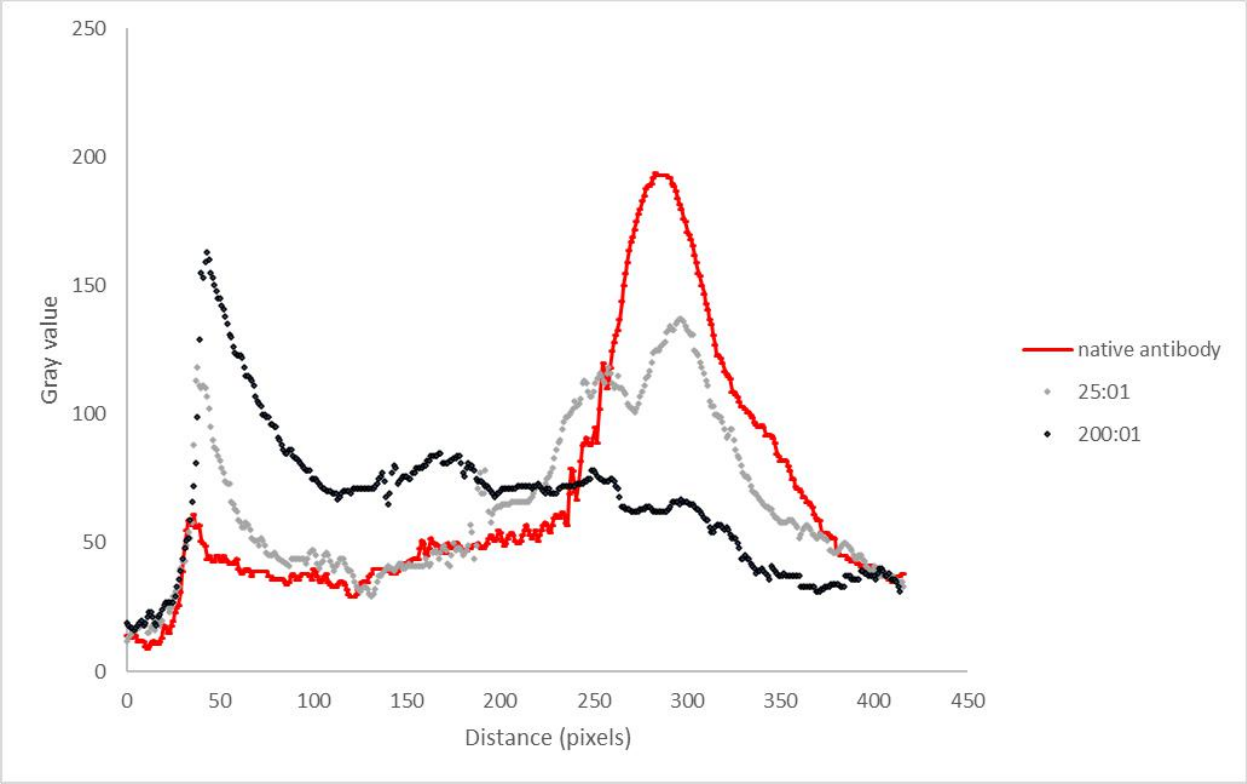


The staining intensity of lane 1, 5, 9 were analyzed by Image J, in which they were converted to Gray value (vertical axis), the location of stains was converted to Distance (horizontal axis), with the direction from top to bottom. Comparing the conjugate synthesized by 200:1 pNIPAAm/antibody ratio to the conjugate synthesized by 25:1 pNIPAAm/antibody ratio, the stain was much less intense at native antibody location, indicating more antibody being conjugated with polymer.

Supplemental figure 2.3.2.1: SDS-PAGE after thermal-precipitation

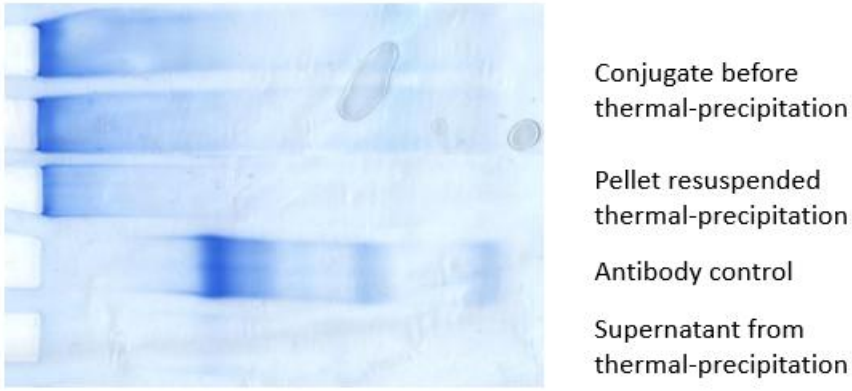


Supplemental figure 2.3.2: HPLC standards

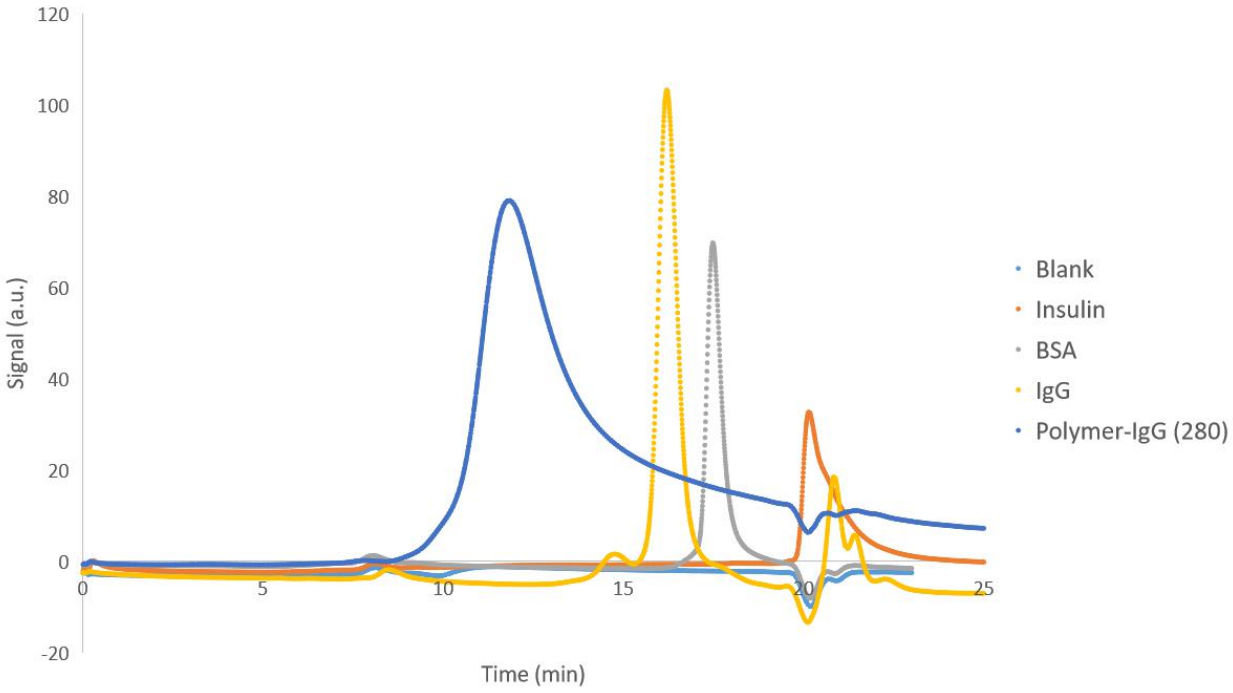

# Chapter 3. EXTRACELLULAR VESICLE SEPARATION VIA BINARY REAGENT SYSTEM

## 3.1 INTRODUCTION

### 3.1.1 *Placental Extracellular Vesicles*

The human pregnancy, a complicated mode of reproduction, starts from the fertilization where the female egg cell fuses with the male gamete. After the fertilization occurred in one of the two fallopian tubes, the fertilized egg would move towards uterus. During the journey, a rapid rate of cell division makes the fertilized egg develop into a blastocyst. When the blastocyst settles down on a place on the maternal endometrium, which is called implantation, becomes the biogenesis of placenta. Upon the implantation of blastocyst, the outer layer of blastocyst develops into trophoblasts, which is considered as the outer layer of placenta. In terms of the cell type, the trophoblast can be divided into two layers. The overlying layer is called syncytiotrophoblast (STB), which is a multi-nucleated cell layer that penetrates the maternal endometrium and establishes an interface between maternal blood and embryonic extracellular fluid. The underlying layer is called cytotrophoblast, where the cells will differentiate and fuse into the overlying layer during the pregnancy period. During human pregnancy, placenta can provide crucial support to the fetus including hormonal, nutritional, oxygen and immunological support. In addition, the signal substances and immunoregulatory factors secreted from placenta can actively modulate the maternal immune response. [25]

Despite its importance, we still know little about placenta. Especially, the previous researches mainly focused on the organ after delivery instead of studying it during pregnancy. As a result, hard to monitor the placental development and functions in real time becomes one of the current barriers to predict pregnancy outcomes and develop interventions. Recently, the rapid growth of extracellular vesicle researches illuminates the strategy to use placental EVs to assess pregnancy in real time. Placental EVs potentially provide non-invasive markers for abnormal placental development.

Placental exosomes, released from syncytiotrophoblast, are functioning in the fetal–maternal crosstalk for adaptation of the maternal organism to the ongoing pregnancy.[25] The Syncytiotrophoblast (STB) is the primary source of placenta derived EV. With specific STB markers, principally placental alkaline phosphatase (PLAP), we are able to distinguish STB derived EV (STBEV) from those produced by other cell types.[26] During pregnancy, these Syncytiotrophoblast membrane microparticles (STBM)-derived exosomes and circulating vesicles from other cells (endothelial cells, platelets, leukocytes, erythrocytes) consist the complex population of circulating EVs in placenta. These circulating extracellular vesicles are closely related to the processes such as coagulation, endothelial dysfunction, immune modulation and inflammation, which could potentially lead to abnormal or complicated pregnancies.[27]

Pre-eclampsia is defined as new onset hypertension (systolic blood pressure of higher than 140 mm Hg and diastolic blood pressure of higher than 90 mm Hg), proteinuria (more than 300 mg).

Pre-eclampsia is reported to occur in approximately 5~7% of pregnant women globally and is a major cause of maternal and neonatal morbidity and mortality.[28] Many researches have been conducted to shed light on the correlation between placenta-derived exosomes and pre-eclampsia state. Pillay.P *et al* suggest the differences in the contribution of placental-derived exosomes to total exosomes in maternal circulation infers a possible pathophysiological role of placental-derived exosomes in pre-eclampsia.[28] Salomon.C *et al* suggest the concentration and content of exosomes may be of diagnostic utility for women at risk for developing PE even if the role of exosomes during PE is not fully elucidated.[29] Gilani, Sarwat I. *et al* also suggest changes in the concentrations and contents of placental EVs may contribute to the pathophysiology of preeclampsia.[30]

## 3.2 Material and Methods

### 3.2.1 *Materials*

Reagents:

Qiazol lysis buffer and MiniElute RNA extraction kit were purchased from Qiagen. Taqman advanced miRNA assay kit was purchased from Thermo Fisher Scientific.

### 3.2.2 *Seminal EV Preparation*

The collection and pre-isolation of seminal EVs was done as reported by Lucia in 2014.[31] The fluorescent labeling of sEV was done as follows. Add 2.5ul DiI dye into 100uL sEV, vortex to mix well. Place the tube in darkness for 60 minutes. Add all incubated sEV into an Amicon Ultra 100k tube, add PBS buffer to dilute the sEV solution to 15ml. Centrifuge the Amicon tube at 3700rpm for 30 minutes. Discard the flow-through. Repeat the washing. Collect the concentrate in the membrane. Even though excess DiI dye should flow through the membrane, some dye may aggregate or form dimers, thus stay in the membrane. Therefore, the DiI-sEV solution may contain some free DiI dyes.

### 3.2.3 *EV separation*

Except for sEV separation, other types of EV separation were using the same protocol. The total volume of EV separation reaction in each tube was fixed at 600uL, in which EV sample took 50% of total volume (300uL), mNPs (10mg/mL) took 10% of total volume (60uL), sodium chloride (2M) took 10% of total volume (60uL). Generally, the amount of antibody for EV markers was 5ug, and the conjugate would apply 10:1 conjugate/antibody ratio. If the target is purified sEV, the total volume would use 300uL, in which sEV volume was 50uL, mNPs (10mg/mL) took 10% of total volume (30uL), sodium chloride (2M) took 10% of total volume (30uL). Also, the amount of antibody for EV markers was 5ug. In a typical sEV separation, 50uL DiI-labeled sEV were mixed with 0.11uM antibody in 300uL final volume.

At first, the antibody was added into the EV sample, gently vortex to mix well. Then, incubate the solution for 30 minutes. After the incubation, the conjugate was added into the solution and would use another 30-minute incubation. Add the mNPs and salt at last, quickly vortex and spin down the solution. Set the tubes in 40°C water bath for 10 minutes, and then perform magnetic separation under the same condition. Carefully collect all the supernatant, then resuspend the captured portion by PBS or lysis buffer for storage or downstream analysis. In this study, 700uL Trizol or Qiazol lysis buffer was added to the captured portion to resuspend the EVs, 3x volume of lysis buffer was added to the supernatant portion. The resuspended captured portion and supernatant should be stored under -20°C or -80°C.

### 3.2.4 *RNA extraction*

The captured portion from magnetic separation was resuspended in 700uL Qiazol lysis buffer. For 700μL resuspended sample, add 140μL chloroform into the sample tube. Shake (do not vortex) vigorously for 15 seconds. Incubate for 3 minutes at room temperature. Centrifuge the samples for 15 minutes at 12,000 xg at 4°C. Transfer the upper aqueous phase to new microcentrifuge tube. (Do not disturb the organic phase.) Use pipet to measure the aqueous phase volume and add 1.5x volume of 100% ethanol. Assemble MinElute spin column in a new collection tube. Load up to 700ul of mixture including any precipitate that may have formed onto the column. Spin for 30 seconds at 1,000 xg at room temperature. Discard the flow-through. Repeat the loading the spinning steps until entire sample has been loaded. Add 700ul buffer RWT to the RNeasy MinElute Spin column. Centrifuge for 30 seconds at 8,000 xg at room temperature to wash the column. Discard the flow-through. Pipet 500ul buffer RPE onto the

RNeasy MinElute spin column. Centrifuge for 30 seconds at 8,000 xg to wash the column. Discard the flow-through. Pipet 500ul fresh 80% ethanol onto RNeasy MinElute spin column. Centrifuge for 2 minutes at 8,000 xg at room temperature to wash the column. Discard the collection tube with the flow-through. Transfer the RNeasy into a new collection tube. Open the lid of the spin column, centrifuge at full speed for 5 minutes to dry the membrane. (Label the tube since the lids can break off) Discard the collection tube with the flow-through. Transfer the RNeasy MinElute spin column in a new collection tube. Add 18ul of RNase-Free water directly onto the center membrane. Centrifuge for 1 min at 10,000 rpm to elute RNA.

### 3.2.5 *Taqman Advanced miRNA Assays*

The eluted RNA from EV samples were processed by following the standard protocol of Taqman advanced miRNA assays kit. The assays comprised 4 steps: Poly(A) tailing, Adaptor ligation, Reverse transcription and miR-Amp reaction. After Reverse transcription step was completed, the cDNA product could be stored at -20°C for up to 2 months. Run miR-Amp reaction before the downstream digital droplet PCR or qPCR. In miR-Amp step, half amount of sample and buffer would be enough (2.5uL cDNA and 22.5uL Master Mix).

### 3.2.6 *ddPCR*

Calculate the total reaction numbers for each cDNA [(sample# + 1 non-template control + 2 overage) x 2 (for duplicate)]. Prepare enough reagents and samples according to the total reaction numbers and the table (Supplemental figure 3.2.6). Dilute the miR-Amp product to 5x

by water before mixing the reagents. (Dilute reverse transcription reagents so they would not inhibit PCT amplification, and assure the DNA concentration was not too high to cause signal saturation)

### 3.2.7 *qPCR*

Calculate the total reaction numbers for each cDNA [(sample# + 1 non-template control + 2 overage) x 2 (for duplicate)]. Dilute the miR-Amp product to 10x by water before mixing the reagents. Prepare reagents and samples according to the total reaction numbers and the table (Supplemental figure 3.2.7), quickly vortex and spin down. The thermal cycling is programmed as shown in Supplemental figure 3.2.8.

## 3.3 Results and Discussion

### 3.3.1 *Seminal EV separation by targeting tetraspanins*

*Seminal EV separation by targeting tetraspanins*

In the study, seminal EV was the first target analyte for EV separation tryout. Human semen is an easy biological fluid to collect and is a complex mixure, like we expect all EVs from biological fluids to be, so in this way is more complex than EV from cell cultures. And our colleagues had successfully got high yields and high concentrations seminal EV from semen related researches.[31] In order to target seminal EV, tetraspanin antibodies were used in this study.

Tetraspanin is a transmembrane protein family which plays a critical role in cell biology and physiology. Among tetraspanins, CD9, CD63, CD81 are specially enriched in the membrane of exosomes[32], and thus are frequently used as exosome biomarkers. In this section, the isolated EVs from human semen were known to contained high concentration of CD9, CD63 and CD81. Thus, a combination of three anti-tetraspanin antibodies was used to select seminal EVs (sEV) via binary reagent system, while the mouse IgG isotype control which should not capture sEV was used as the control antibody.

The seminal EVs in the study were labelled with DiI, a lipophilic membrane fluorophore, for the detection before and after EV separation. The fluorescent intensity of the post-separation supernatant, which positively related to the amount of uncaptured EVs, was used to evaluate the separation. Figure 3.3.1 showed the fluorescent measurement data from 5 DiI-sEV separation trials. A combination of CD9, CD63 and CD81 antibody was used for the sEV selection in the first group and mouse IgG isotype control was used as a control antibody in the second group. For the normalization, an extra group was prepared by simply diluting the same amount of sEV to the same total volume as the other groups. The fluorescent intensity from the normalization group was 100% since all DiI-sEV was in the supernatant. Based on the conjugate binding characterization, 1.1 – 1.65μM anti-mouse IgG conjugate (10:1 – 15:1 conjugate:antibody molar ratio) was used for the separations. In figure 3.3.1, to facilitate the comparison across different trials, the fluorescent intensity in each trial was converted to percentage by normalizing to the normalization group in each trial. Across multiple trials, the background noise, measured by PBS buffer, was no more than 0.5% of the full signal. By comparing using the tetrespanin antibody with using control antibody, the tetraspanin antibody led to lower fluorescent intensity in

supernatant (22.66%, averaged from 5 trials) while the mouse IgG control antibody led to higher fluorescent intensity in supernatant (41.70%, averaged from 5 trials). All 5 trials shared the same trend that the mouse IgG control group had higher fluorescent signal in supernatant compared to tetraspanin antibody group. Since the fluorescent signal came from the DiI dye labeled on sEV, the higher fluorescent signal in supernatant portion indicated more DiI-sEV being captured by antibody, the lower fluorescent signal in supernatant portion indicated less DiI-sEV being captured by antibody. Taken together, these data suggested that using tetraspanin antibody would result in higher DiI-sEV capture compared to using control antibody, confirming the tetraspanin antibody-mediated specific sEV selection via binary reagent system. Other EV separations in this study utilized a set of DiI-sEV separation as control experiment to confirm the reagents and separation protocol were working as expected. Note that the fluorescent data were not meant to be used for quantitating the separation efficiency but just to give an estimate to show the trend. Many situations, such as the unlabeled circulating DiI dye in solution and interaction between DiI and smart reagents could cause the gap between the fluorescent signal and the real sEV quantity.

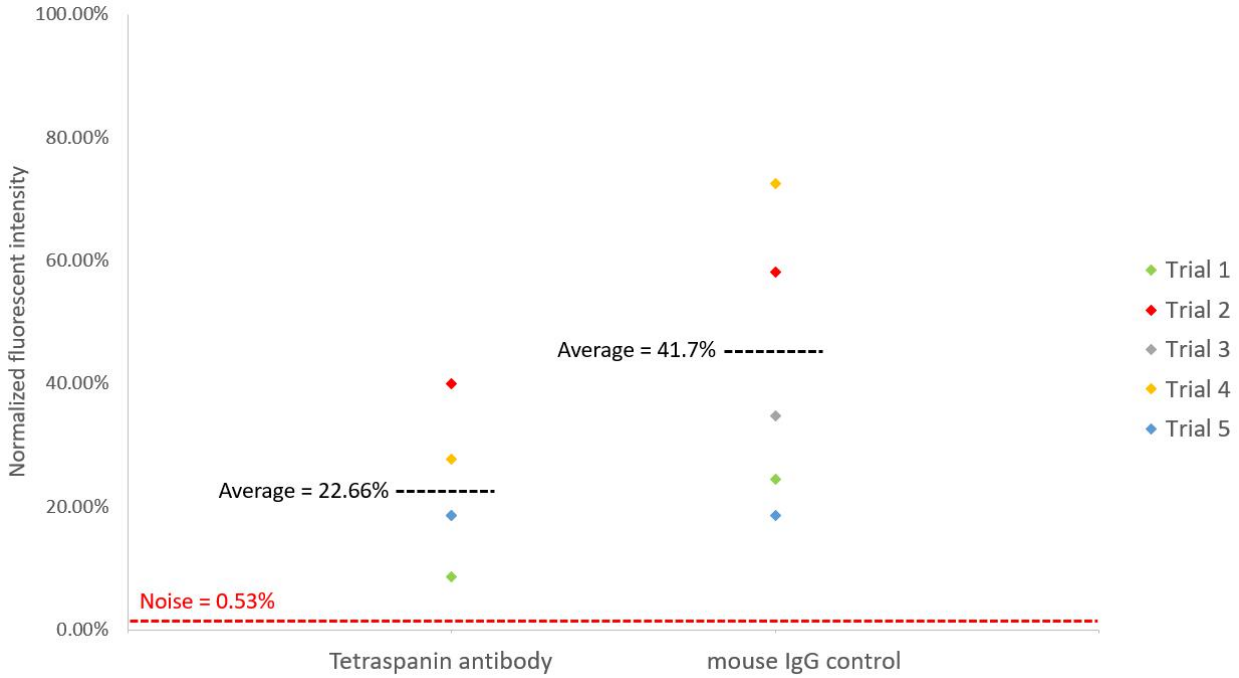


Figure 3.3.1: 5 DiI-sEV separations characterized by fluorescent measurement.

In 5 separated sEV separation trials, the capture efficiency of tetraspanin antibody and control antibody via binary reagent system was compared. The raw fluorescent intensity from tetraspanin group and control group was converted to percentage by normalizing to a dilution group, which was simply prepared by diluting the same amount of DiI-sEV to the same total volume as the other two groups. The averaged noise, 0.53%, was measured by normalizing the raw fluorescent intensity from PBS buffer groups to the dilution group. This noise indicated that the background signal generated by buffer was insignificant. From these 5 different trials, the tetraspanin groups, in average, were having lower fluorescent intensity in supernatant, meaning more DiI-sEV being captured (data points from trial 3 and trial 5 in tetraspanin group were overlapped with each other). And the control antibody groups, in average, were having higher fluorescent intensity in supernatant, meaning less DiI-sEV being captured. These data suggested

that using tetraspanin antibody to select DiI-sEV resulted in higher sEV capture efficiency compared to using control antibody.

In addition to DiI-sEV, the separation was also evaluated by detecting miRNAs enclosed in the EV using RT-PCR. This approach is more time consuming but can potentially quantitate the separation. After the separation, the captured EV or the supernatant were mixed with lysis buffer for the downstream RNA extraction and detection. At the same time, constant amount of cel39 was spiked into each sample as a control miRNA for RNA extraction process as well as the subsequent reverse transcription and DNA amplification. The raw data from RT-PCR were the cycle threshold (Ct) values from each group. The Ct value is generally defined as the number of cycles required for the fluorescent signal from a positive reaction to reach a determined threshold. As a result, the higher Ct means more cycles to reach the fluorescence threshold, indicating a lower starting concentration of the target DNA. On the other hand, lower Ct indicates a higher starting target DNA concentration. However, the Ct values cannot be used to quantitate RNA or cDNA concentration directly, since the RNA extraction process, or the amplification efficiency in RT-PCR across different groups could be different. In other words, even if there was identical amount of RNA or cDNA in two different groups, it might turn out that they had different absolute Ct value after RT-PCR due to the different RNA extraction process or RT-PCR amplification efficiency. As a result, we need to add a normalizer miRNA into each group before RNA extraction to control the process of RNA extraction as well as the subsequent RT-PCR. In this study, cel39 was used as the normalizer miRNA to control the RNA extraction, reverse transcription, and amplification. In the RT-PCR, both the target miRNA and the control miRNA were reverse transcribed and amplified. The absolute Ct values from both target miRNA and

control miRNA need to be taken into calculation for quantitation. Since the concentration of control miRNA was identical across each group, the first step to quantitate target miRNA was to normalize the target miRNA Ct value against control miRNA Ct value. The △Ct, meaning the difference beten target miRNA Ct and control miRNA Ct, was calculated by target miRNA Ct value minus cel39 Ct value. The △Ct of a target miRNA meant how much more cycles did this target miRNA need to reach the fixed threshold comparing to the control miRNA. As a result, a higher △Ct meant the target miRNA needed more amplification cycles to reach the concentration threshold, indicating a lower target miRNA concentration, while a lower △Ct meant less amplification cycles needed to reach the concentration threshold, indicating a higher target miRNA concentration. Thus, we were able to compare the same target miRNA concentration in two different experimental conditions simply by comparing their △Ct in the two experimental groups. When it came to the sEV separation mediated by tetraspanin antibody, the tetraspanin group was expected to have a lower △Ct because more captured sEV would lead to higher target miRNA concentration in the capture portion. And the control antibody group was expected to have a higher △Ct because less captured sEV would lead to lower target miRNA concentration in captured portion. Figure 3.3.2 shows the results from RT-PCR of 3 sEV separation trials. According to preliminary researches from our colleagues, let-7b, miR-148a, let-7a, miR-375 and miR-99a were known to be abundant in seminal EVs.[31] Among those, two seminal specific miRNAs, let-7b and/or miR-375, were used for characterizing these sEV separations. In these experiments, the captured portion went through RNA extraction and RT-PCR and was analyzed by the method described above. Trial 1 only used let-7b as target miRNA, trial 2 only used miR-375 as target miRNA, trial 3 used both let-7b and miR-375 as target miRNAs. For each trial, the target miRNAs were normalized to cel39 control miRNA

respectively. The data in figure 3.3.2 showed that all 4 sets of data from 3 independent trials exhibited lower △Ct in tetraspanin antibody group compared to mouse IgG control antibody group, which was in good agreement with the expected results. This trend meant that using tetraspanin antibody would lead to higher seminal specific miRNA concentration in captured portion, compared to using the mouse IgG control antibody, indicating higher sEV capture by tetraspanin antibodies. In conclusion, the data from these experiments confirmed specific sEV separation mediated by the tetraspanin antibodies via binary reagent system. Note that, it was not recommended to compare the △Ct across different trials (e.g. trials from different dates or trials using different reagents, instrument or protocols), since these trials might have differences in template, reaction mix, protocol and instrument configuration, resulting in absolute Ct differences even if using the same miRNA target.

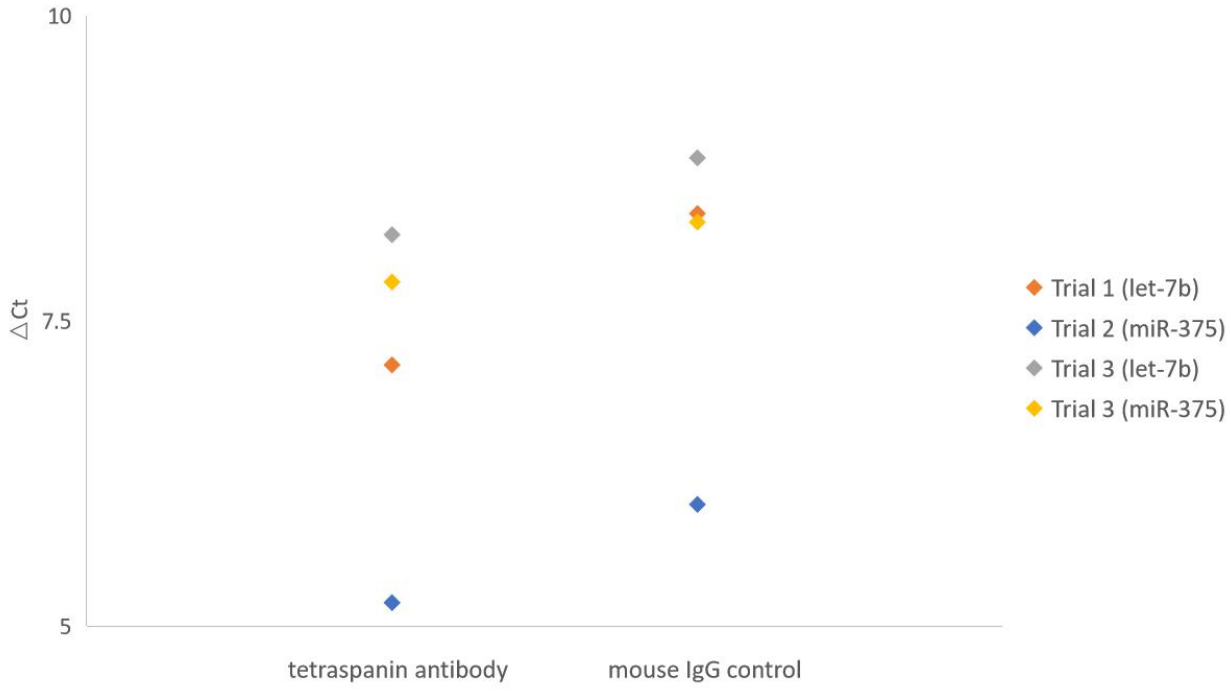

Figure 3.3.1.2: RT-PCR characterizing 4 SEV separation trials.

The figure compared the relative target miRNAs (let-7b and/or miR-375) concentration in captured portion from tetraspanin antibody group and control antibody group. The direct Ct values of let-7b or miR-375 were normalized to control miRNA to generate △Ct. The higher △Ct meant lower target miRNA concentration while the lower △Ct meant higher target miRNA concentration. Trial 1 only used let-7b as target miRNA, trial 2 only used miR-375 as target miRNA, trial 3 used both let-7b and miR-375 as target miRNAs. Taken the data from all the trials together, we observed a clear trend that the tetraspanin antibody group had lower △Ct than control antibody group. This result suggested that using tetraspanin antibodies to select sEV via binary reagent system would lead to higher seminal specific miRNAs concentration in captured portion than using control antibody.

### 3.3.2 *Perfusion EV separation by targeting placental alkaline phosphatase (PLAP)*

The specific syncytiotrophoblast marker, placental alkaline phosphatase (PLAP) is exclusively expressed in placenta derived EVs among all kinds of EVs.[33] In this chapter, the PLAP antibody for perfusion EV separation was provided by colleagues from Oxford[34, 35]. The perfusion EV used in the experiment was pre-isolated and purified by the protocol reported by R.A.Dragovic from Oxford in 2015.[36] The prepared perfusion EV was spiked in buffer and male plasma before starting the experiments. After EV separation, the RNAs were extracted from the samples. In order to identify suitable miRNA markers for perfusion EV characterization, a pilot sequencing study was conducted. In total 5 different samples, including human plasma from healthy males,

normal pregnant females, pre-eclampsia females, non-pregnant females as well as pre-isolated and purified perfusion EV were separation by PLAP antibody via binary reagent system. Both the supernatants and captured portions after EV separation were collected for pilot sequencing. Among multiple miRNAs being examined, miR1323 and miR517 were two miRNAs abundant in captured portion from pregnancy plasma and were absent in male plasma. As a result, the two placental specific miRNAs, miR1323 and miR517a were chosen as miRNA marker for quantitation through quantitative RT-PCR and digital droplet PCR (ddPCR) for separation characterization.

Figure 3.3.2.1 showed ddPCR characterization of perfusion EV spiked in male plasma separation. In the experiment, 5μg of PLAP antibody or mouse IgG isotype control was mixed with the sample firstly, followed by adding anti-mouse IgG conjugate. Based on the conjugate binding characterization, 1.1μM or 1.65μM anti-mouse IgG conjugate (10:1 or 15:1 conjugate:antibody molar ratio) were used in the pEV separation. After separation, the RNA was extracted and reverse transcribed. Digital droplet PCR (ddPCR) was used to quantitate the concentration of miR1323 and miR517a in both captured portion and supernatant. The raw data from ddPCR were target miRNA concentration (copies/μL). Since the perfusion EVs were prepared from human placenta, all of them were expected to express PLAP on their surface. Thus, the PLAP antibody should be able to recognize and capture highest amount of pEV from the sample via binary reagent system. The tetraspanins, CD9, CD63 and CD81 were also predominantly existed on the surface of perfusion EVs as introduced in chapter 2. Therefore, using the combination of 3 tetraspanin antibodies should be able to recognize and capture most of the pEV from the samples via binary reagent system. The tetraspanin antibody-selected pEV and PLAP antibody-selected pEV might have comparable concentration. The control antibody which did not recognize any of

the pEV should not have any positive signal in captured portion. Figure 3.3.2.1a showed the miR1323 concentration from PLAP antibody group, tetraspanin (CD9 + CD63 + CD81) antibody group and mouse IgG control group. The captured series showed that using PLAP antibody to select pEV resulted in highest miR1323 concentration, using 3 tetraspanin antibodies combination (CD9, CD63, CD81) to select pEV resulted in slightly lower miR1323 concentration, while using control antibody to select pEV resulted in the lowest miR1323 concentration. The miR1323 concentration in supernatant portions showed a reverse trend, which correlated with the results from the captured portion. Taken the two series together, PLAP antibody enabled higher pEV captured from male plasma background, compared with mouse IgG control and tetraspanin antibody. Figure 3.3.2.1b showed the characterization via miR517a. However, the fluorescent signals from the captured portion of tetraspanin antibody group and PLAP antibody group were too high to fit in the detection range of detector. If I were to show the captured portion signal from tetraspanin antibody group and PLAP antibody group in the figure, they would be off the charts and would make it hard to read. But note that even if we were not able to compare the tetraspanin antibody group and PLAP antibody group because their signal saturate the detector, but we knew that both tetraspanin antibody group and PLAP antibody group had significant higher signal intensity than control antibody group because the signal from control antibody group was reasonably detectable by the detector. Thus, the figure 3.3.2.1b only showed the signal from the antibody-depleted supernatants of the 3 groups. In this figure, miR517a signal from supernatant portions clearly showed the same trend that mouse IgG control group had highest signal intensity in supernatant while PLAP antibody group and tetraspanin antibody group had comparable signal intensity with each other and were both lower than control antibody group. This observation was in good agreement with the signal from miR1323.

Combining two sets of data from miR1323 and miR517a (Supplemental figure 3.3.2.1) together, it was confirmed that the pEV separation was specifically mediated by PLAP antibody from male plasma background via binary reagent system.

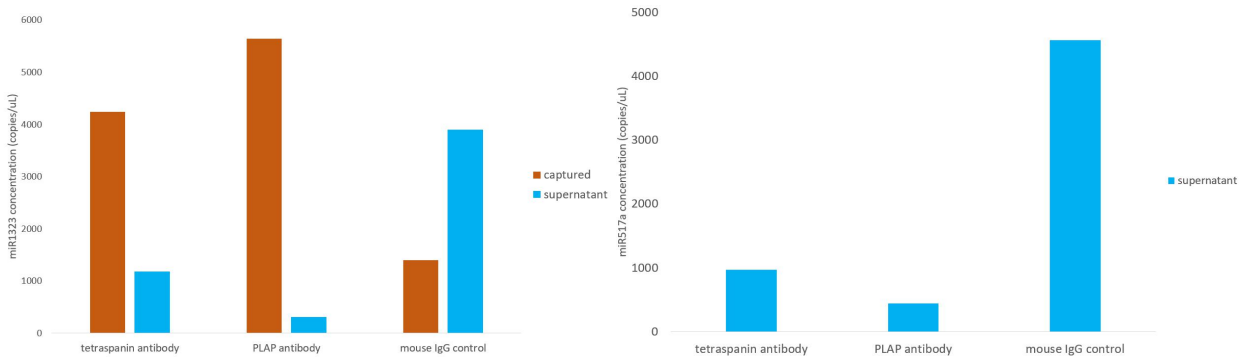


miR1323 miR517a

Figure 3.3.2.1: ddPCR characterization of pEV spiked in male plasma separation (Left: miR1323, Right: miR517a).

Figure 3.3.2.1 Left showed the miR1323 concentration from PLAP antibody group, tetraspanin (CD9+CD63+CD81) antibody group and mouse IgG control group. The brown bars showed the miR1323 concentration from captured portion. The PLAP antibody group had the highest miR1323 concentration, the tetraspanin antibody group had slightly lower miR1323 concentration, while the control antibody group had the lowest miR1323 concentration. This trend indicated that using PLAP antibody realized highest perfusion EV capture compared to using tetraspanin antibody and using control antibody. The blue bars showed the miR1323 concentration from antibody-depleted supernatants. We could observe that the control antibody group had the most miR1323 left in the supernatant, while the PLAP antibody group had the least miR1323 in supernatant. The miR1323 concentration trends from 3 supernatants and 3

captured portions were in good agreement, confirming the specific perfusion EV separation mediated by PLAP antibody via binary reagent system. Figure 3.3.2.1 Right showed the characterization done by the other target miRNA, miR517a. The signals from the 3 captured portions were not shown in this figure since the miR517a concentration from tetraspanin antibody group and PLAP antibody group were beyond the upper limit of the detector, and were certainly much higher than the miR517a concentration in control antibody group. The blue bars showed the miR517a signals from 3 supernatant portions, which clearly displayed the same trend as shown by miR1323. The control antibody group had highest miR517a concentration in supernatant, while PLAP antibody group and tetraspanin antibody group had comparable miR517a concentration and were both much lower than control antibody group. The miR517a characterization result was in good agreement with the miR1323 characterization result (figure 3.3.2.1a).

To further confirm the result from ddPCR characterization, the pEV separation was repeated for RT-PCR characterization. The separation was using the same samples and was conducted according to the same protocol. The tetraspanin antibody group was removed in the repeated experiments. After EV separation, the RNAs were extracted from the samples by following the same steps. Subsequently, the same target miRNAs, miR1323 and miR517a, were quantitated through quantitative RT-PCR. Figure 3.3.2.2 showed the RT-PCR characterization of captured portion from perfusion EV spiked in male plasma separation by targeting placental specific miRNA. The raw data from RT-PCR were Ct values, which could be readily transformed to $\triangle$Ct as described in 3.3.2.1. In short, a lower $\triangle$Ct value indicated higher target miRNA concentration while a higher $\triangle$Ct indicated lower target miRNA concentration. As explained above, the PLAP

antibody group was expected to have the highest miRNA concentration in the captured portion, corresponding to the lowest △Ct. The control antibody group was expected to have the lowest miRNA concentration in captured portion, corresponding to the highest △Ct. The RT-PCR data from 3 independent trials were plotted and were displayed in figure 3.3.2.2. It was clearly showed that, in 3 separate trials, the PLAP antibody groups were all having lower △Ct compared to mouse IgG control group, meaning using PLAP antibody to select pEV resulted in higher placental specific miRNA concentration in captured portion while comparing to using mouse IgG control antibody. Thus, the same trend from RT-PCR data shared by 3 independent trials confirmed the PLAP antibody-mediated isolation of $PLAP^+$ EV from pEV-spiked male plasma via binary reagent system.

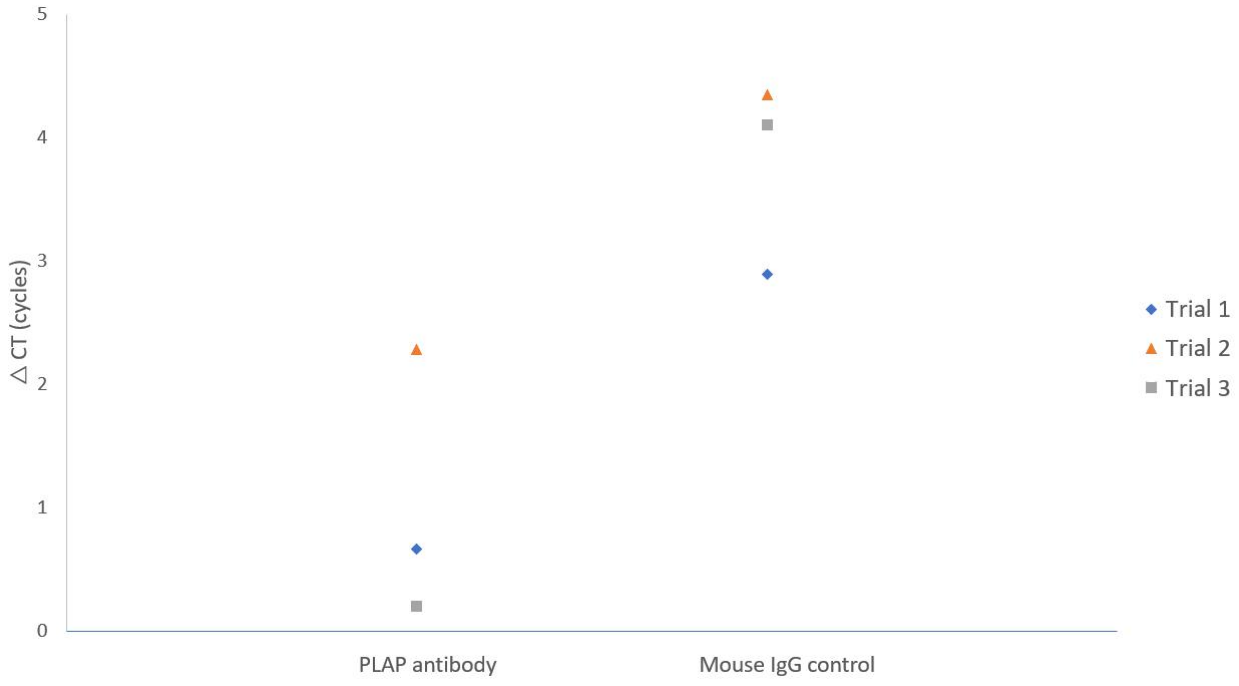


Figure 3.3.2.2: RT-PCR characterization of pEV spiked in male plasma separation.

This figure showed the △Ct comparison of miR1323 or miR517a concentration between PLAP antibody group and control antibody group. The higher △Ct value indicated the lower target miRNA concentration, while the lower △Ct value indicated the higher target miRNA concentration. From 3 independent trials, all the PLAP antibody groups were showing significantly lower △Ct than corresponding control antibody groups. This trend meant that using PLAP antibody to select pEV from male plasma via binary reagent system resulted in higher pEV capture than using control antibody.

### 3.3.3 *Isolating placental derived EV by targeting placental alkaline phosphatase (PLAP)*

To further confirm the specific placental EV separation from human plasma, we used PLAP antibody and control antibody on human pregnancy plasma separation via binary reagent system. In the separation, we followed the same EV separation protocol and used the same PLAP antibody provided from our colleagues as in perfusion EV separation. After EV separation, the RNAs were extracted from the samples. The same placental-specific miRNAs, miR1323 and miR517a, were used for placental EV quantitation through quantitative RT-PCR. Since the human pregnancy plasma was a complex sample which contained multiple types of EVs from different parental cells, using tetraspanin antibodies would capture all kinds of EVs with tetraspanins on surface. Thus, only PLAP antibody and mouse IgG isotype control were used in human pregnancy plasma separation. The analysis of RT-PCR data was the same as described in chapter 3.3.2. The direct Ct values of miR1323 and miR517a were normalized against the control miRNA cel39, which derived △Ct for comparing the same target miRNA across

different experimental groups. As explained in chapter 3.3.2, a higher △Ct indicated lower miRNA concentration while a lower △Ct indicated higher miRNA concentration. Thus, the PLAP antibody should be able to recognize and capture placental EVs due to their surface PLAP expression from pregnancy plasma via binary reagent system. The control antibody which did not recognize any of the EVs from pregnancy plasma should not capture anything from pregnancy plasma. Figure 3.3.3a showed the comparison of miR1323 concentration in captured portions from PLAP antibody group and mouse IgG control group. In two independent trials, we observed the identical trend that PLAP antibody group had significant lower △Ct compared to control antibody group. This trend meant that the miR1323 concentration in PLAP antibody-selected portion was significantly higher than the miR1323 concentration in control antibody-selected portion. Figure 3.3.3b showed the comparison of miR517a concentration in captured portions from PLAP antibody group and mouse IgG control group. From the same trials, we observed the same trend that PLAP antibody group had significant lower △Ct compared to control antibody group, leading to the same conclusion as the miR1323 characterization. Taken two placental-specific miRNA characterization together, we could conclude that using PLAP antibody enabled specific placental EVs isolation via binary reagent system.

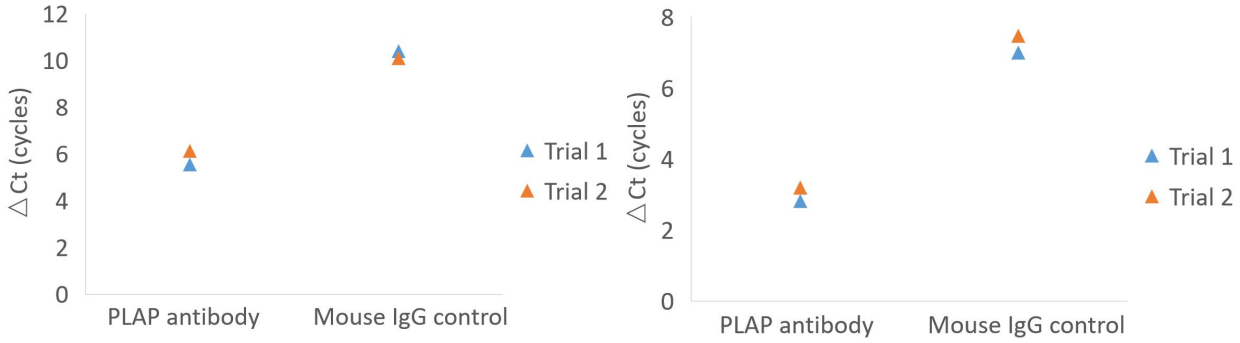


Figure 3.3.3: RT-PCR characterization of human pregnancy plasma separation (miR1323 and miR517a).

Left figure showed the miR1323 characterization of pregnancy plasma separation mediated by PLAP antibody and control antibody. The direct Ct values of miR1323 were converted to △Ct by normalizing against control miRNA cel39. Data from two independent trials displayed a same trend that the PLAP antibody groups were having significantly lower △Ct compared to control antibody group, indicating higher miR1323 concentration in PLAP antibody captured portion than in control antibody captured portion. Right figure showed the miR517a characterization for the same trials. The miR517a characterized △Ct from PLAP antibody groups and control antibody groups displayed the same trend as in miR1323 characterization. The data from two placental-specific miRNAs were in good agreement and confirmed the specific placental EV separation mediated by PLAP antibody via binary reagent system.

## 3.4 SUPPLEMENTAL INFORMATION

Supplemental figure 3.2.6: ddPCR reaction

| Component | 1 Rxn (uL) |
|---|---|
| ddPCR SuperMix 2X | 11 |

| | |
|---|---|
| Each primer probe | 1.1 |
| Water | 7.4 |
| Sample | 2.5 |
| Total | 22 |

Supplemental figure 3.2.7.1: qPCR reaction

| Components | 1 Rxn (uL) |
|---|---|
| 2X qPCR Master Mix | 7.5 |
| 20X Primer | 0.75 |
| cDNA | 6.75 |
| total | 15 |

Supplemental figure 3.2.7.2: qPCR thermal cycling program

| Step | Temperature (°C) | Time | Cycles |
|---|---|---|---|
| Hold stage | 50 | 2 min | 1 |
| | 95 | 10 min | 1 |
| PCR stage | 95 | 15 sec | 40 |

| | | | |
|---|---|---|---|
| | 60 | 1 min | |
| | 4 | Hold | 1 |

Supplemental figure 3.3.2.1: ddPCR characterization of pEV spiked in buffer separation

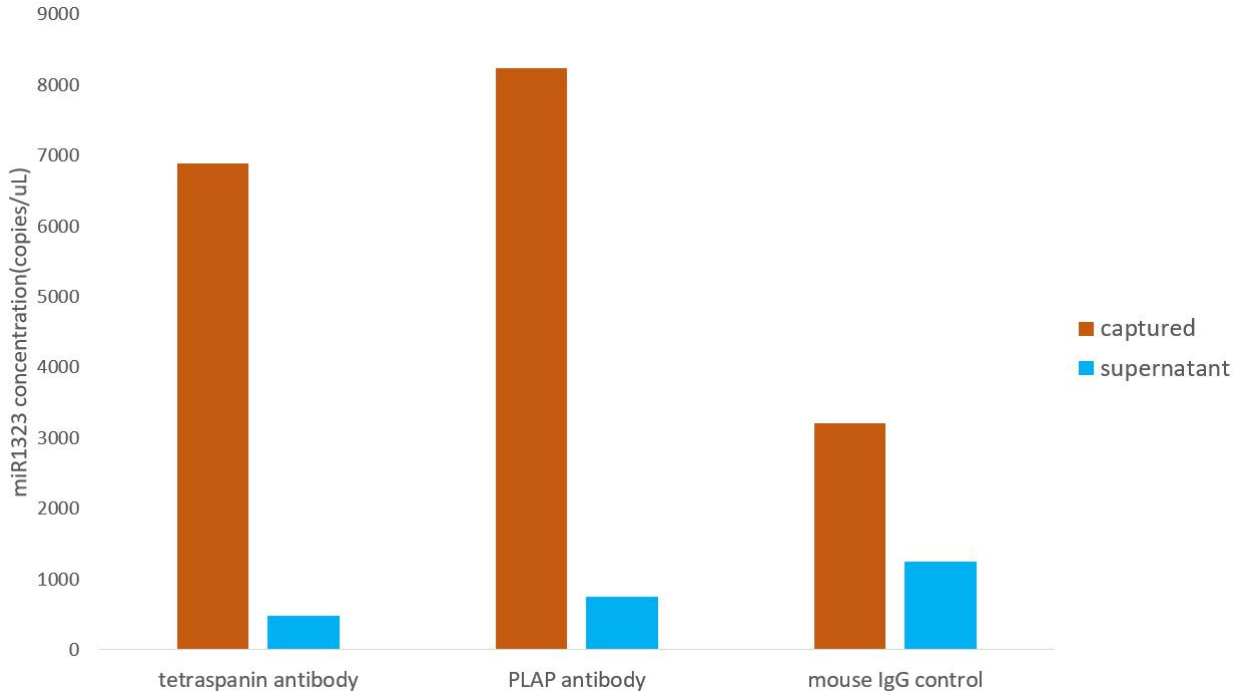

# BIBLIOGRAPHY


1. EL Andaloussi, S.; Maeger, I.; Breakefield, X. O.; Wood, M. J. A., Extracellular vesicles: biology and emerging therapeutic opportunities. *Nat Rev Drug Discov* **2013,** *12* (5), 348-358.
2. Yanez-Mo, M.; Siljander, P. R. M.; Andreu, Z.; Zavec, A. B.; Borras, F. E.; Buzas, E. I.; Buzas, K.; Casal, E.; Cappello, F.; Carvalho, J.; Colas, E.; Cordeiro-da Silva, A.; Fais, S.; Falcon-Perez, J. M.; Ghobrial, I. M.; Giebel, B.; Gimona, M.; Graner, M.; Gursel, I.; Gursel, M.; Heegaard, N. H. H.; Hendrix, A.; Kierulf, P.; Kokubun, K.; Kosanovic, M.; Kralj-Iglic, V.; Kramer-Albers, E. M.; Laitinen, S.; Lasser, C.; Lener, T.; Ligeti, E.; Line, A.; Lipps, G.; Llorente, A.; Lotvall, J.; Mancek-Keber, M.; Marcilla, A.; Mittelbrunn, M.; Nazarenko, I.; Nolte-t' Hoen, E. N. M.; Nyman, T. A.; O'Driscoll, L.; Olivan, M.; Oliveira, C.; Pallinger, E.; del Portillo, H. A.; Reventos, J.; Rigau, M.; Rohde, E.; Sammar, M.; Sanchez-Madrid, F.; Santarem, N.; Schallmoser, K.; Ostenfeld, M. S.; Stoorvogel, W.; Stukelj, R.; Van der Grein, S. G.; Vasconcelos, M. H.; Wauben, M. H. M.; De Wever, O., Biological properties of extracellular vesicles and their physiological functions. *J Extracell Vesicles* **2015,** *4*.
3. Xu, X. B.; Lai, Y. Y.; Hua, Z. C., Apoptosis and apoptotic body: disease message and therapeutic target potentials. *Bioscience Rep* **2019,** *39*.
4. Raposo, G.; Stoorvogel, W., Extracellular vesicles: Exosomes, microvesicles, and friends. *J Cell Biol* **2013,** *200* (4), 373-383.
5. Whiteside, T. L., Tumor-Derived Exosomes and Their Role in Tumor-Induced Immune Suppression. *Vaccines-Basel* **2016,** *4* (4).
6. Balusu, S.; Van Wonterghem, E.; De Rycke, R.; Raemdonck, K.; Stremersch, S.; Gevaert, K.; Brkic, M.; Demeestere, D.; Vanhooren, V.; Hendrix, A.; Libert, C.; Vandenbroucke, R. E., Identification of a novel mechanism of blood-brain communication during peripheral inflammation via choroid plexus-derived extracellular vesicles. *Embo Mol Med* **2016,** *8* (10), 1162-1183.
7. Yu, Y.; Gool, E.; Berckmans, R. J.; Coumans, F. A. W.; Barendrecht, A. D.; Maas, C.; van der Wel, N. N.; Altevogt, P.; Sturk, A.; Nieuwland, R., Extracellular vesicles from human saliva promote hemostasis by delivering coagulant tissue factor to activated platelets. *J Thromb Haemost* **2018,** *16* (6), 1153-1163.
8. Karnati, H. K.; Garcia, J. H.; Tweedie, D.; Becker, R. E.; Kapogiannis, D.; Greig, N. H., Neuronal Enriched Extracellular Vesicle Proteins as Biomarkers for Traumatic Brain Injury. *J Neurotraum* **2019,** *36* (7), 975-987.
9. Fiandaca, M. S.; Kapogiannis, D.; Mapstone, M.; Boxer, A.; Eitan, E.; Schwartz, J. B.; Abner, E. L.; Petersen, R. C.; Federoff, H. J.; Miller, B. L.; Goetzl, E. J., Identification of preclinical Alzheimer's disease by a profile of pathogenic proteins in neurally derived blood exosomes: A case-control study. *Alzheimers Dement* **2015,** *11* (6), 600-607.
10. Kim, S. H.; Lechman, E. R.; Bianco, N.; Menon, R.; Keravala, A.; Nash, J.; Mi, Z. B.; Watkins, S. C.; Gambotto, A.; Robbins, P. D., Exosomes derived from IL-10-treated dendritic cells can suppress inflammation and collagen-induced arthritis. *J Immunol* **2005,** *174* (10), 6440-6448.
11. Szatanek, R.; Baran, J.; Siedlar, M.; Baj-Krzyworzeka, M., Isolation of extracellular vesicles: Determining the correct approach (Review). *Int J Mol Med* **2015,** *36* (1), 11-17.
12. Andreu, Z.; Rivas, E.; Sanguino-Pascual, A.; Lamana, A.; Marazuela, M.; Gonzalez-Alvaro, I.; Sanchez-Madrid, F.; de la Fuente, H.; Yanez-Mo, M., Comparative analysis of EV isolation procedures for miRNAs detection in serum samples. *J Extracell Vesicles* **2016,** *5*.
13. Li, X.; Corbett, A. L.; Taatizadeh, E.; Tasnim, N.; Little, J. P.; Garnis, C.; Daugaard, M.; Guns, E.; Hoorfar, M.; Li, I. T. S., Challenges and opportunities in exosome research-Perspectives from biology, engineering, and cancer therapy. *Apl Bioeng* **2019,** *3* (1).
14. Konoshenko, M. Y.; Lekchnov, E. A.; Vlassov, A. V.; Laktionov, P. P., Isolation of Extracellular Vesicles: General Methodologies and Latest Trends. *Biomed Res Int* **2018**.
15. Carnino, J. M.; Lee, H.; Jin, Y., Isolation and characterization of extracellular vesicles from Broncho-alveolar lavage fluid: a review and comparison of different methods. *Resp Res* **2019,** *20* (1).
16. Haq, M. A.; Su, Y.; Wang, D., Mechanical properties of PNIPAM based hydrogels: A review. *Mater Sci Eng C Mater Biol Appl* **2017,** *70* (Pt 1), 842-855.
17. Schmaljohann, D., Thermo- and pH-responsive polymers in drug delivery. *Adv Drug Deliver Rev* **2006,** *58* (15), 1655-1670.
18. Bi, J. J.; Song, K. D.; Wu, S. L.; Zhang, Y.; Wang, Y. W.; Liu, T. Q., Effect of thermal-responsive surfaces based on PNIPAAm on cell adsorption/desorption. *Int J Polym Mater Po* **2019,** *68* (4), 145-151.
19. Lanzalaco, S.; Armelin, E., Poly(N-isopropylacrylamide) and Copolymers: A Review on Recent Progresses in Biomedical Applications. *Gels* **2017,** *3* (4).
20. Kumar, A.; Srivastava, A.; Galaev, I. Y.; Mattiasson, B., Smart polymers: Physical forms and bioengineering applications. *Prog Polym Sci* **2007,** *32* (10), 1205-1237.
21. Jones, D. S.; Lorimer, C. P.; Mccoy, C. P.; Gorman, S. P., Characterization of the physicochemical, antimicrobial, and drug release properties of thermoresponsive hydrogel copolymers designed for medical device applications. *J Biomed Mater Res B* **2008,** *85b* (2), 417-426.
22. M.S.Uddin, N. S. L. H. K. H., Thermosensitive polymer coated nanomagnetic particles for separation of bio-molecules. *Separation and purification technology* **2007,** *53.2*, 164-170.
23. Nehilla, B. J.; Hill, J. J.; Srinivasan, S.; Chen, Y. C.; Schulte, T. H.; Stayton, P. S.; Lai, J. J., A Stimuli-Responsive, Binary Reagent System for Rapid Isolation of Protein Biomarkers. *Anal Chem* **2016,** *88* (21), 10404-10410.
24. Jauregui, R.; Srinivasan, S.; Vojtech, L. N.; Gammill, H. S.; Chiu, D. T.; Hladik, F.; Stayton, P. S.; Lai, J. J., Temperature-Responsive Magnetic Nanoparticles for Enabling Affinity Separation of Extracellular Vesicles. *Acs Appl Mater Inter* **2018,** *10* (40), 33847-33856.
25. Mincheva-Nilsson, L.; Baranov, V., The Role of Placental Exosomes in Reproduction. *Am J Reprod Immunol* **2010,** *63* (6), 520-533.
26. Tannetta, D.; Masliukaite, I.; Vatish, M.; Redman, C.; Sargent, I., Update of syncytiotrophoblast derived extracellular vesicles in normal pregnancy and preeclampsia. *J Reprod Immunol* **2017,** *119*, 98-106.
27. Toth, B.; Lok, C. A. R.; Boing, A.; Diamant, M.; van der Post, J. A. M.; Friese, K.; Nieuwland, R., Microparticles and exosomes: Impact on normal and complicated pregnancy. *Am J Reprod Immunol* **2007,** *58* (5), 389-402.

28. Pillay, P.; Maharaj, N.; Moodley, J.; Mackraj, I., Placental exosomes and pre-eclampsia: Maternal circulating levels in normal pregnancies and, early and late onset pre-eclamptic pregnancies. *Placenta* **2016,** *46*, 18-25.
29. Salomon, C.; Guanzon, D.; Scholz-Romero, K.; Longo, S.; Correa, P.; Illanes, S. E.; Rice, G. E., Placental Exosomes as Early Biomarker of Preeclampsia: Potential Role of Exosomal MicroRNAs Across Gestation. *J Clin Endocr Metab* **2017,** *102* (9), 3182-3194.
30. Gilani, S. I.; Weissgerber, T. L.; Garovic, V. D.; Jayachandran, M., Preeclampsia and Extracellular Vesicles. *Curr Hypertens Rep* **2016,** *18* (9).
31. Vojtech, L.; Woo, S.; Hughes, S.; Levy, C.; Ballweber, L.; Sauteraud, R. P.; Strobl, J.; Westerberg, K.; Gottardo, R.; Tewari, M.; Hladik, F., Exosomes in human semen carry a distinctive repertoire of small non-coding RNAs with potential regulatory functions. *Nucleic Acids Res* **2014,** *42* (11), 7290-7304.
32. Kowal, J.; Arras, G.; Colombo, M.; Jouve, M.; Morath, J. P.; Primdal-Bengtson, B.; Dingli, F.; Loew, D.; Tkach, M.; Thery, C., Proteomic comparison defines novel markers to characterize heterogeneous populations of extracellular vesicle subtypes. *Proc Natl Acad Sci U S A* **2016,** *113* (8), E968-77.
33. Tannetta, D.; Collett, G.; Vatish, M.; Redman, C.; Sargent, I., Syncytiotrophoblast extracellular vesicles - Circulating biopsies reflecting placental health. *Placenta* **2017,** *52*, 134-138.
34. Cronqvist, T.; Tannetta, D.; Morgelin, M.; Belting, M.; Sargent, I.; Familari, M.; Hansson, S. R., Syncytiotrophoblast derived extracellular vesicles transfer functional placental miRNAs to primary human endothelial cells. *Sci Rep-Uk* **2017,** *7*.
35. Cooke, W. R.; Cribbs, A.; Zhang, W.; Kandzija, N.; Motta-Mejia, C.; Dombi, E.; Ri, R.; Cerdeira, A. S.; Redman, C.; Vatish, M., Maternal circulating syncytiotrophoblast-derived extracellular vesicles contain biologically active 5 '-tRNA halves. *Biochem Bioph Res Co* **2019,** *518* (1), 107-113.
36. Dragovic, R. A.; Collett, G. P.; Hole, P.; Ferguson, D. J.; Redman, C. W.; Sargent, I. L.; Tannetta, D. S., Isolation of syncytiotrophoblast microvesicles and exosomes and their characterisation by multicolour flow cytometry and fluorescence Nanoparticle Tracking Analysis. *Methods* **2015,** *87*, 64-74.